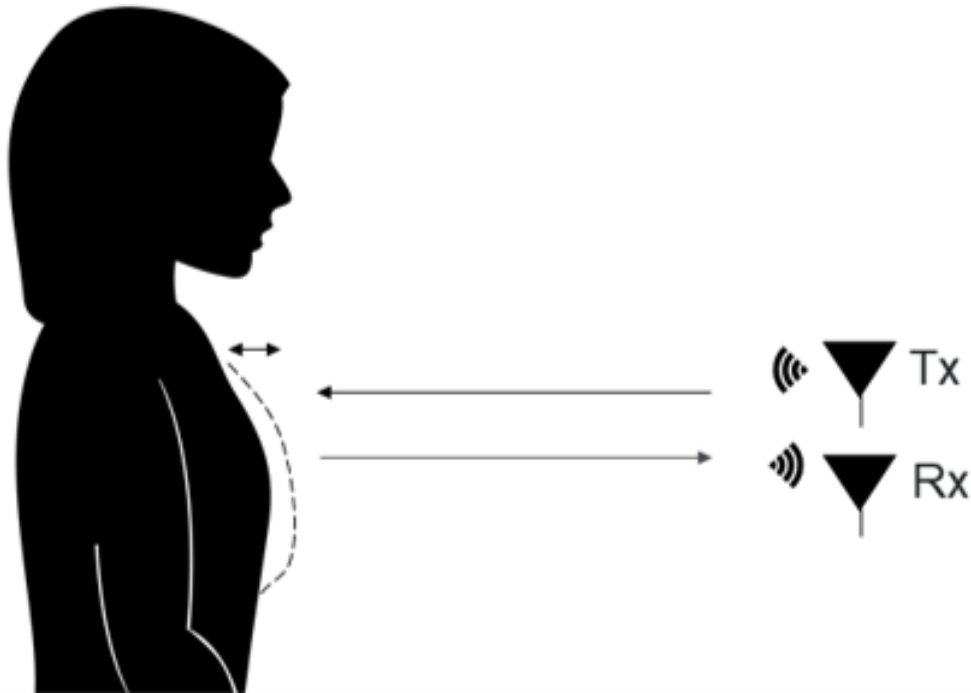
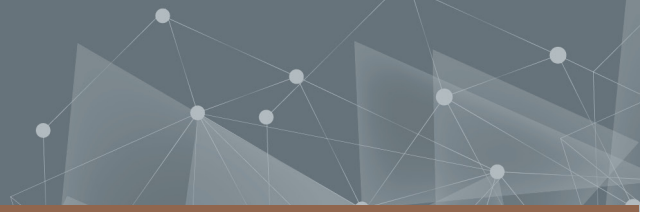




CHALMERS
UNIVERSITY OF TECHNOLOGY



Radar Based In-Vehicle Health Monitoring

Using FMCW Radar for Breathing and Heartbeat Detection

Master's Thesis in Biomedical Engineering

OSKAR ANDERSSON
JULIA NYSTRAND

DEPARTMENT OF ELECTRICAL ENGINEERING

CHALMERS UNIVERSITY OF TECHNOLOGY
Gothenburg, Sweden 2021
www.chalmers.se

MASTER'S THESIS 2021

Radar Based In-Vehicle Health Monitoring

Using FMCW Radar for Breathing and Heartbeat Detection

OSKAR ANDERSSON
JULIA NYSTRAND



CHALMERS
UNIVERSITY OF TECHNOLOGY

Department of Electrical Engineering
Division of Signal Processing and Biomedical Engineering
Biomedical Electromagnetics
CHALMERS UNIVERSITY OF TECHNOLOGY
Gothenburg, Sweden 2021

Radar Based In-Vehicle Health Monitoring
Using FMCW Radar for Breathing and Heartbeat Detection
Oskar Andersson
Julia Nystrand

© Oskar Andersson, Julia Nystrand, 2021.

Supervisors: Xuezhi Zeng, Department of Electrical Engineering
Johan Karlsson, Autoliv

Co-supervisor: Ke Lu, Department of Electrical Engineering

Examiner: Xuezhi Zeng, Department of Electrical Engineering

Master's Thesis 2021
Department of Electrical Engineering
Division of Signal Processing and Biomedical Engineering
Biomedical Electromagnetics
Chalmers University of Technology
SE-412 96 Gothenburg
Telephone +46 31 772 1000

Cover: Vital sign measurements using a radar, further described in section 2.2.

Typeset in L^AT_EX
Printed by Chalmers Reproservice
Gothenburg, Sweden 2021

Radar Based In-Vehicle Health Monitoring
Using FMCW Radar for Breathing and Heartbeat Detection
Oskar Andersson, Julia Nystrand
Department of Electrical Engineering
Chalmers University of Technology

Abstract

Systems for detecting driver sleepiness is a highly relevant field to prevent traffic accidents. Current solutions use indirect measurements, e.g. of the driver's steering movements, the car's position in its lane, or systems based on eye tracking. Adding measurements of physiological signals such as breathing rate (BR) and heart rate (HR) allow more exact detection of sleepiness. However, measuring physiological signals usually require electrodes attached to the subject. In the context of driving, a contactless solution is of interest. In this project a radar-based approach is investigated to measure HR and BR, without the need of direct body contact.

Several potential integration solutions are available. Here, the feasibility of measuring from a seat belt position is investigated, along with initial testing from the steering wheel. The project also includes an analysis of the impact of parameters such as vibrations from the car, movements of the driver, talking etc. Data has been collected from a test setup in a vibration rig, with the purpose of simulating real driving. The collected data has been further processed in order to extract BR and HR information. Signal processing involve band pass filtering, wavelet analysis, moving mean filtering and peak detection. The results of the project show that average BR and HR can be measured accurately for a stationary test subject. However, the robustness to distortions such as vibrations and movements of the subject is still a challenge. Further work is suggested to focus on the measurement setup, ensuring a high quality signal as well as how to handle individual differences in BR and HR.

Keywords: sleepiness detection, driver monitoring, radar, FMCW, breathing rate, heart rate, wavelets, moving average, peak detection

Acknowledgements

First of all, we would like to express our gratitude for getting the opportunity to participate in this project. It has been a rewarding and interesting time, full of new insights and knowledge.

Special thanks to our Chalmers supervisor, Xuezhi Zeng, for your support, always answering all our questions and helping out when needed. All the time with a positive and happy attitude, spreading joy.

We would also like to thank our Autoliv supervisor, Johan Karlsson, for your support and guidance during the project and for solving all practical issues. We appreciate that you always contribute with new ideas and make sure to push us and the project forward.

Further, we would like to thank our co-supervisor, Ke Lu, for adding valuable input to the project, often with new, interesting perspectives.

We also appreciate all the help from Autoliv, both with practical issues related to the data collection, as well as input on the signal processing. Special thanks to Magnus Ekerås, for all the help with setting up the vibration rig and always being very helpful.

Last but not least, we would like to thank our opponents, Henrik Pettersson and Olivia Stensöta, for an interesting discussion and all the feedback on the report.

Oskar Andersson & Julia Nystrand
Gothenburg, June 2021

Contents

Abstract	v
Acknowledgements	vii
List of Figures	xi
List of Tables	xiii
List of Abbreviations	xiv
1 Introduction	1
1.1 Background	1
1.2 Aim and Goals	3
1.3 Method	4
1.4 Delimitations	4
1.5 Outline of the Thesis	5
2 Theory	7
2.1 Frequency Modulated Continuous Wave Radar	7
2.1.1 Detection of Small Movements	9
2.2 Radar-Based Physiological Measurements	10
2.2.1 Reflection and Penetration Depth	10
2.3 Signal Processing of Radar Signal	11
2.3.1 Demodulation Techniques	11
2.3.1.1 Classic Demodulation	11
2.3.1.2 Linear Demodulation	13
2.3.2 Wavelet Analysis	14
2.3.2.1 Basic Concept	14
2.3.2.2 Adjustable Parameters for Signal Processing	16
2.3.3 Moving Average Filtering	16
3 Methods	17
3.1 Equipment	17
3.1.1 Radar Configuration	18
3.2 Data Collections	18

3.2.1	Test Setup	19
3.2.2	Data Collection 1	20
3.2.3	Data Collection 2	21
3.3	Data Processing and Analysis	21
3.3.1	Demodulation and Range Bin Selection	22
3.3.2	Baseline Drift Removal	23
3.3.3	Filtering to Extract Heartbeats and Breathing	24
3.3.4	Peak Detection and Average Heart Rate and Breathing Rate Calculations	25
3.3.5	Signal Processing of the Reference Data	25
3.3.6	Evaluation	26
3.4	Heart Sound Detection	26
4	Results	27
4.1	Results for Different Test Conditions	27
4.1.1	Stationary Test Subject	27
4.1.2	Impact of Steering Movements	30
4.1.3	Performance with Vibrations	32
4.1.4	Effects of Talking	34
4.1.5	Measurements Wearing a Jacket	35
4.2	Results Related to Signal Processing	36
4.2.1	Comparison of Wavelet Analysis and Moving Average Filtering	36
4.2.2	Cut-off Frequency of Band Pass Filter	39
4.2.3	Performance of Linear Demodulation	40
4.3	Additional Results	41
4.3.1	Detection of Heart Sounds	41
4.3.2	Steering Wheel Measurements	42
5	Discussion	45
5.1	Evaluation of Different Test Conditions	45
5.2	Analysis of Test Setup	47
5.3	Hardware and Radar Configuration	49
5.4	Individual Differences Between Subjects	50
5.5	Feasibility of Measuring Heart Sounds	51
5.6	Discussion of Signal Processing	51
5.6.1	Future Signal Processing	52
5.7	Ethical Considerations	52
6	Conclusion	55
	References	57
A	Summary of Data Collections	I

List of Figures

2.1	Visual representations of a chirp as magnitude-time plot in (a) and frequency-time plot in (b).	7
2.2	Schematic view of the FMCW radar operations.	8
2.3	Visualisation of vital sign monitoring using a radar.	10
2.4	The process of classic demodulation	11
2.5	Example of a range-FFT with peaks corresponding to objects in front of the radar.	12
2.6	Example of wrapped and unwrapped phase.	12
2.7	The process of linear demodulation	13
2.8	Visualisation of linear demodulation. (a) Raw I/Q data. (b) DC component removed. (c) Demodulated data.	14
2.9	Example of a wavelet shape (Symlet 6).	15
2.10	Block diagram of wavelet decomposition for DWT. The components included in the final decomposition are marked by dashed lines.	15
3.1	The radar hardware used. (a) Texas Instruments AWR1642BOOST (b) Texas Instruments DCA1000EVM.	17
3.2	NeXus-10 MKII. Image used with permission [28].	18
3.3	Test setup with driver seat and steering wheel mounted on a vibrating rig.	19
3.4	Antenna locations during data collection; steering wheel (a) and seat belt (b).	20
3.5	Block diagram of the general steps of the signal processing.	22
3.6	Example of range bin selection, red cross representing a detection.	22
3.7	Example of signal with baseline drift (a) and after removal (b) using the wavelet approach.	23
4.1	Average BR ((a) and (c)) and HR ((b) and (d)) for two test cases where the test subjects are sitting still. (a) and (b) are from the same test, and the same applies for (c) and (d).	28
4.2	Demodulated radar signal for four different measurements with the same test conditions and subject. The test condition is without vibrations and movements.	29
4.3	Demodulated radar signal (a) and average BR (b) when test subject start small steering movements.	31

4.4	Demodulated radar signal from two different tests with steering movements.	31
4.5	Average BR (a) and HR (b) for the signal shown in Figure 4.4a.	32
4.6	Examples of demodulated radar signals from measurements with motorway vibrations.	33
4.7	Average BR for the signal in Figure 4.6a in (a) and for the signal in Figure 4.6b in (b).	33
4.8	The effects of talking. Here, the breathing pattern is disrupted when the subject says the days of the week in a calm pace.	34
4.9	Average BR for a measurement when the subject had a conversation during the complete measurement.	35
4.10	(a) Average BR and (b) HR for a case where the subject wore a jacket. Here, also vibrations were applied.	36
4.11	Average BR ((a) and (c)) and HR ((b) and (d)) for two test cases where the test subjects are sitting still. (a) and (b) are from the same test case, and the same applies for (c) and (d). Here, the wavelet method is used for signal processing.	37
4.12	Average BR ((a) and (c)) and HR ((b) and (d)) for two test cases where the test subjects are sitting still. (a) and (b) are from the same test case, and the same applies for (c) and (d). Here, the signal processing is a combination of the wavelet approach and the moving average filter.	38
4.13	Average HR for two tests with different subjects, when the lower cut-off frequency in the band pass filter used for baseline drift removal, is set to 0.8 Hz. The subjects are sitting still, and there are no vibrations applied. The test cases are the same as in (a) Figure 4.1d, and (b) Figure 4.1b.	40
4.14	(a) Radar signal demodulated using linear demodulation, same data as in Figure 4.2a. (b) Corresponding linearly demodulated I/Q data.	41
4.15	Estimated BR for the same test as shown in Figure 4.14 when using (a) linear demodulation, and (b) classic demodulation.	41
4.16	Heart sounds shown as a blue line. The red vertical lines are the reference ECG signal.	42
4.17	The IBI of the heart sounds and the reference ECG, for the measurement shown in Figure 4.16.	42
4.18	(a) Average BR and (b) HR from a measurement conducted from the steering wheel.	43

List of Tables

3.1	Signal processing parameters.	24
4.1	Summary of accuracy of signals shown in Figure 4.2.	29
4.2	Summary of accuracy for BR and HR when test subject sit still.	30
4.3	Summary of accuracy for measurements with small steering movements from the test subject, during the whole test.	32
4.4	Summary of accuracy for measurements with motorway vibrations.	34
4.5	Summary of accuracy for measurements during a conversation.	35
4.6	Summary of accuracy for measurements with the subject wearing a jacket. For all cases the subject is sitting still, but vibrations are applied.	36
4.7	Summary of accuracy of signals shown in Figure 4.11, where the wavelet approach is used for signal processing.	38
4.8	Summary of accuracy of signals shown in Figure 4.12, where a combination of wavelets and moving average filters is used for signal processing.	39
4.9	Summary of accuracy on signals shown in Figure 4.1, where the moving average filter is used alone for the signal processing.	39
A.1	Summary of test cases for the first data collection.	I
A.2	Sequence with events, applied during first test collection.	II
A.3	Summary of test cases for the second data collection.	II

List of Abbreviations

ADC Analog-to-Digital Converter.

BPM Beats per Minute, Breaths per Minute.

BR Breathing Rate.

DC Direct Current.

DWT Discrete Wavelet Transform.

ECG Electrocardiography.

FFT Fast Fourier Transform.

FMCW Frequency Modulated Continuous Wave.

HRV Heart Rate Variability.

HR Heart Rate.

IBI Inter Breath Interval, Inter Beat Interval.

RMS Root Mean Square.

1

Introduction

In this chapter a background to the project is given, putting it in a wider context. An overview of previous research in the area is presented, followed by the aim and goals of this project. The methods used are briefly described as well as the delimitations that have been set. Lastly, the outline of this report is defined.

1.1 Background

Improving traffic safety is important to minimise traffic accidents and prevent severe injuries and deaths. Statistics from the World Health Organisation [1] state that the number of deaths due to traffic accidents continue to increase, reaching 1.35 million deaths in 2016. This places deaths from traffic accidents as the 8th leading cause of death globally, among all ages. The reason for an accident can be various, but studies show that sleepiness can be an important factor in 10 to 40 percent of the cases [2]. The National Highway Traffic Safety Administration, part of the United States Department of Transportation, reported that in 2017 almost 800 people were killed as a result of sleepy drivers [3]. The fact that this is a vast problem has led to innovations that try to mitigate the issue. One such is the development of advanced driver-assistance systems (ADAS) that try to detect and predict sleepiness of the driver. In fact, the European Commission recently updated their regulations, making driver sleepiness detection a mandatory safety feature in new cars from 2022 [4].

Several different approaches to measure driver sleepiness are used today. In [5] the methods are divided into subjective, vehicle-based, behavioural, physiological, and hybrid methods.

Subjective methods are in general based on questionnaires for the subject to assess their sleepiness. Gathering this type of measurements during real-time driving is commonly used in research. But in an end-user product, these methods are not an option.

Further on, vehicle-based methods are based on characteristics for accidents where sleepy drivers are involved. Measurements of the driving patterns and how the driver

control the vehicle on the road are used to detect potential sleepy drivers. According to [5], two of the most common types of vehicle-based methods for detecting sleepiness are steering-wheel movement and standard deviation of lane position. The steering-wheel movement method uses an angle sensor that detect steering movements. When the driver is sleepy, small corrections in the steering are more unlikely. However, this approach often produces many false positives. The standard deviation of lane position method uses a camera to monitor the car's position in its lane. Drifting around in the lane or out of it are typical signs of a sleepy driver. For this to work, factors such as road marking, weather and lighting conditions must be sufficiently good.

The behaviour of the driver could also be monitored in order to detect sleepiness. Usually this is done with a camera monitoring the drivers head and face during driving. Factors such as facial expression, yawning, the head and eye position and the state of the eyes are all suggested to be used for detecting sleepiness. According to [5] these systems are cost effective and non-invasive which is an advantage. However, designing systems like this require advanced computer vision and face recognition. Another challenge described is bumpy roads and changes in lightning that occur during real-time driving.

The use of physiological methods enables objective and more exact measurements of sleepiness. These methods utilise physiological signals, which start to change in the early stages of sleepiness. Two physiological signals mentioned in [5] are electrocardiogram (ECG) and electroencephalogram (EEG). The ECG signal describe the electrical activity of the heart and from which the heart rate (HR) and heart-rate variability (HRV) can be derived to assess the sleepiness. The EEG signal describe the electrical activity of the brain and this is the most reliable measurement of the alertness of a human. However, EEG is done by attaching electrodes to the scalp of the subject, and this is not feasible in an end-user product. In [6], another physiological signal is used to detect sleepiness, namely the respiration. More specifically, the breathing rate (BR) and the respiratory-rate variability are used to detect sleepiness.

Lastly, [5] point out that efforts are made to combine the different methods described above into hybrid methods, utilising several of their respective benefits. Technical progress can also enable new measurement methods that potentially reduce some of the downsides.

In this thesis efforts are made to develop a contactless, physiological method for measuring the driver's BR and HR based on radar-technology, without bringing any discomfort to the driver.

Previous research regarding radar-based methods for monitoring vital signs show promising results [7]. Several different radar types have been used in this research but in this thesis a frequency modulated continuous wave (FMCW) radar will be used. In a recent study [8], this type of radar has been used for a similar application, monitoring vital signs of a driver. In this study, the radar is placed behind the driver,

in the back rest of the seat, showing promising results for measuring BR and the average HR. However, they point out that further work is needed to reduce motion artifacts. Similarly, in [7], random body movements are described as one of the greatest challenges when monitoring vital signs using a radar. Obviously, the driver will move when turning the steering wheel, during acceleration and deceleration etc. This must be considered when processing the signal.

Furthermore, vibrations from the car will also affect the quality of the measured signal. To mitigate this effect, an accelerometer was used in [8] to detect and compensate for vibrations. There are also attempts to expand the monitoring to include other parameters. For example, in [9] the possibilities of a radar-based heart sound detection are explored, showing that it is feasible.

1.2 Aim and Goals

This project is part of a research collaboration between Autoliv and Chalmers University of Technology called Connected Occupant Driver Evaluation (COPE). The COPE project aim to measure, analyse and communicate physiological signals from the driver [10]. Focus is on traffic safety and sleepiness, but also to investigate the possibility to detect acute health conditions, monitor chronic diseases or to adjust rescue responses when there is an accident. The aim of this project is to get insight about the feasibility and the design of a future radar product, but also to inspire to further research and development in the field. As this is a Master's thesis project, the primary goal is to apply current knowledge and also to learn more in the field in order to get a hold of a Master's degree.

The goals of this project are to investigate if a radar based solution for in-vehicle health monitoring could be a potential solution in future traffic safety systems. This includes trying different antenna locations that are suitable for driver monitoring and collecting data from the chosen locations. In the process of selecting relevant antenna locations, preferences from Autoliv will be considered. Further, a data analysis method needs to be developed in order to extract the respiration and heartbeat signal from the collected data.

A summary of the goals is presented below.

- Explore the possibility of measuring HR and BR from antenna positions relevant for Autoliv products, such as steering wheel and seatbelt.
- Develop a data analysis method and evaluate the robustness of the method for different measurement conditions.
- Investigate the possibility of detecting heart sounds using the same test setup.

1.3 Method

This project includes collection of data, processing of it and an evaluation of the results. The data collection was carried out at two separate occasions, the first in the beginning of the project and the second later on. For the first data collection, many parameters were varied, for instance, vibrations were applied, body movements were carried out by the test subjects and different clothing were tested. Furthermore, data from both the seat belt and the steering wheel was collected. The collected data was then processed in order to extract breathing and heartbeat signals. Different signal processing techniques were applied, extracting phase information from the radar data, separating breathing and heartbeat information and detecting peaks.

It was later decided to focus on the seat belt position, and for the second data collection additional measurements from that position were done. Efforts were made to separate the effect of different parameters. Also, adding several measurements for each case to support further analysis. A more comprehensive description of the method is presented in Chapter 3.

1.4 Delimitations

In this project there are many aspects to consider that could be subject for further investigation. However, due to the limited time available and other factors, delimitations are necessary. One delimitation that has been set is that the signal processing is done offline and not in real time. Therefore, the time-performance of algorithms and processing techniques will not be of high priority. For a future product, a fast and reliable signal processing will be important but that will not be of priority in this project.

Due to the limited time available the number of test subjects is restricted to the authors of this report. That is, two test subjects, a male and a female in their early twenties. Optimal would of course be to include more test subjects in different ages and gender. However, that would require a substantial amount of extra work and time.

Furthermore, variables such as length and body shape of the driver will not be considered. Obviously, these variables can be interesting with regards to the seat and wheel position as this can change the position of the radar relative to the body. Also, the body shape may have a high impact on the signal quality. However, because of the low number of test subjects, this is not in the scope of this project.

For the radar setup, it could be of interest to explore the option of using several antennas. This would enable to direct the lobe of the radar but also require more sophisticated radar configuration. In this project, only a single antenna pair is used for acquiring data for initial method development.

1.5 Outline of the Thesis

This report is divided into six chapters. In this first chapter a background to the project is given, together with the aim and goals. Moreover, a short presentation of the method and delimitations is included, as well as this outline of the report.

In Chapter 2, Theory, a technical background of the concepts used is presented. The theory cover the function of an FMCW radar and how it can measure physiological signals. Also, relevant signal processing techniques are described.

In Chapter 3, Method, information about how the project is carried out is outlined. The chapter includes detailed descriptions of, the equipment used, the data collections and the applied signal processing.

In Chapter 4, Results, the outcome of the project is shown. The results illustrate both the effect of different parameters, but also the impact of different signal processing techniques.

In Chapter 5, Discussion, the results are further discussed, and relevant topics are elaborated on. This include evaluation of the parameters that has been varied, the test setup used, and the signal processing. Furthermore, ethical considerations are also discussed.

Finally, the conclusions of this thesis are drawn in Chapter 6, Conclusion.

2

Theory

In this chapter necessary theory is covered. First, the function of an FMCW radar is elaborated, describing how it can be used to detect small vibrations. Further, some background of how a radar can measure physiological signals are given. In the last part of this chapter, theory regarding signal processing are presented. More specifically, explaining the demodulation of the radar signal and the use of wavelet analysis and moving average filtering.

2.1 Frequency Modulated Continuous Wave Radar

The operation principle for all radars is similar. A signal is transmitted from an antenna and reflected back by objects in the surroundings. By measuring the reflected signal, relevant information of the object can be obtained. For an FMCW radar the transmitted signal is called a chirp and can be described as a sinusoidal with a linearly increasing frequency, Figure 2.1a. Another, more convenient way of representing a chirp is by a frequency-time plot, see Figure 2.1b. The most fundamental parameters to describe a chirp is the start frequency, f_c , the bandwidth, B and its duration T_c . Also the slope, $S = \frac{B}{T_c}$, could be used to describe the chirp.

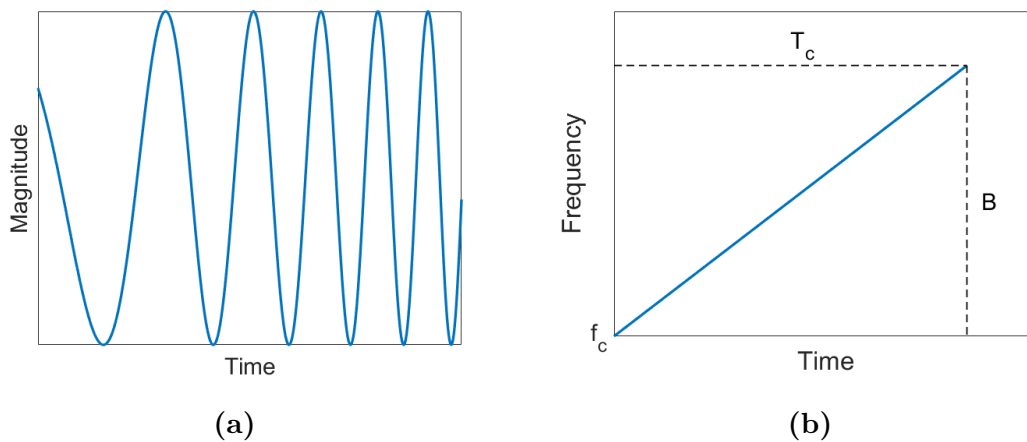


Figure 2.1: Visual representations of a chirp as magnitude-time plot in (a) and frequency-time plot in (b).

In [11] the operation of an FMCW radar is described in four steps, seen in Figure 2.2. First, a chirp is generated by a signal generator. Second, the generated chirp is transmitted by a transmitting antenna. Third, after being reflected on an object, the reflected signal is acquired by the receiving antenna. Lastly, the transmitted and received signal are mixed together, followed by a low pass filter, yielding a signal called intermediate frequency (IF) signal.

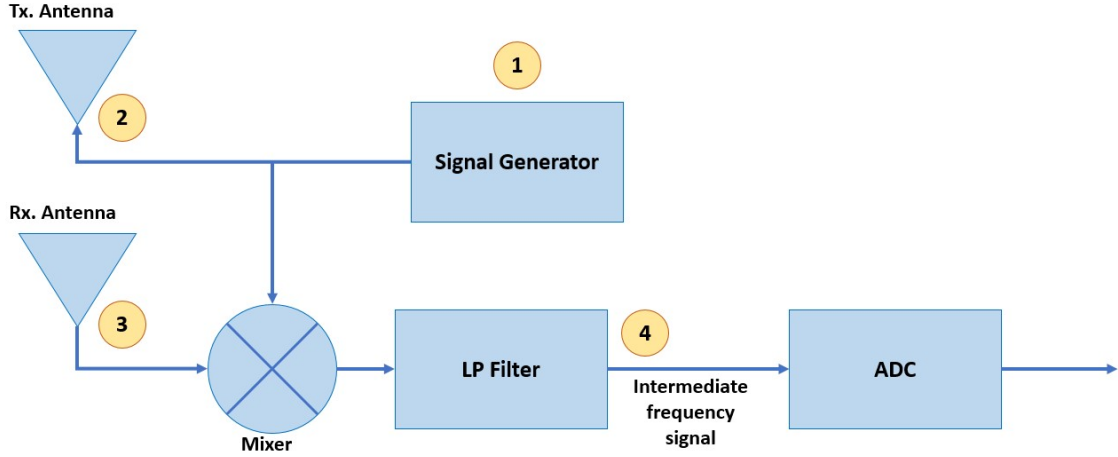


Figure 2.2: Schematic view of the FMCW radar operations.

The operation of an FMCW radar can also be described with mathematics [12]. The transmitted signal, $T(t)$ can be expressed as

$$T(t) = A(t) \sin \left(2\pi \left[f_c t + \frac{B}{2T_c} t^2 \right] \right) \quad (2.1)$$

where $A(t)$ is the voltage amplitude. Assuming a reflection from a distance D_0 , the round trip delay is $t_d = \frac{2D_0}{c}$, with c being the speed of light. The received signal, $R(t)$, can then be expressed as

$$R(t) = B(t) \sin \left(2\pi \left[f_c (t - t_d) + \frac{B}{2T_c} (t - t_d)^2 \right] \right) \quad (2.2)$$

where $B(t)$ is the voltage amplitude. Mixing $T(t)$ and $R(t)$, followed by low pass filtering, yield the IF signal

$$S(t) = C(t) \cos \left(2\pi \left[\frac{2BD_0}{cT_c} t + \frac{2f_c D_0}{c} + \underbrace{\frac{B}{2T_c} \left(\frac{2D_0}{c} \right)^2}_{\approx 0} \right] \right) \quad (2.3)$$

where $C(t)$ is the voltage amplitude. For short distances, the last term in equation (2.3) is close to zero and can be ignored. The resulting IF signal can therefore be expressed as

$$S(t) \approx C(t) \cos \left(2\pi \left[\frac{2BD_0}{cT_c} t + \frac{2f_c D_0}{c} \right] \right). \quad (2.4)$$

From equation (2.4) it can be seen that for a static object, constant D_0 , the IF signal is a sinusoidal with a single frequency. This frequency, f_b , is directly proportional to the distance to the reflected object and given by

$$f_b = \frac{2BD_0}{cT_c} = \frac{2SD_0}{c}. \quad (2.5)$$

Similarly, several objects at different distances from the radar will introduce various frequencies in the IF signal.

As seen in Figure 2.2, the IF signal is also digitised by an analog-to-digital converter (ADC) [11]. The output from the ADC can then be further processed. With equation (2.5) in mind, analysing the frequency content of the ADC signal is a useful way to detect objects in front of the radar. For object detection the range resolution is important. That is how close two objects can be, and still be detected as different objects. The range resolution,

$$d_{res} = \frac{c}{2B}, \quad (2.6)$$

is solely dependent on the bandwidth of the transmitted chirp [11].

2.1.1 Detection of Small Movements

As described above, a moving object will change the frequency of the IF signal. Though, due to the limited bandwidth, small movements of the object will not have a great impact on the frequency. Therefore, small movements cannot be detected only by looking at the frequency content. However, the phase of the IF signal is very sensitive to small movements of the object. The phase, ϕ , is given by the second term in equation (2.4), as

$$\phi = \frac{4\pi f_c D_0}{c} = \frac{4\pi D_0}{\lambda} \quad (2.7)$$

where $\lambda = \frac{c}{f_c}$, is the wavelength [8], [11]. By emitting short chirps closely spaced in time the object can be assumed to be static at the time of reflection and any change of frequency will be negligible. But small movements of the object will be reflected as a change in the phase. For each transmitted chirp, the phase can be calculated and the relative phase, $\Delta\phi$, is given by

$$\Delta\phi = \frac{4\pi f_c \Delta D}{c} = \frac{4\pi \Delta D}{\lambda} \quad (2.8)$$

where ΔD is the small movement of the object. A result of this is that the sampling frequency of the relative phase signal is equal to the frequency that the chirps are transmitted with. It is also worth noting that the sensitivity of the phase is very

high. For a radar operating at 77 GHz, a small movement of 1 mm will introduce a phase change of π radians. Therefore, transmitting a series of chirps, and tracking the change of phase, allow measurements of small movements in the millimeter range. This technique is elaborated further in Section 2.3.

2.2 Radar-Based Physiological Measurements

Radar measurements of the heart and breathing pattern are possible since heartbeats and breathing cause small movements of the chest wall, which are seen as phase changes in the reflected radar signal [13]. The concept is visualised in Figure 2.3. The respiratory displacement of the chest contributes to the signal with larger, slower trends. Normal breathing is within 12 to 20 breaths per minute (BPM), corresponding to frequencies of 0.2 to 0.33 Hz [14]. During inhalation the lungs expand and the distance between chest and the radar antenna decrease, and the opposite applies for exhalation. The amplitude of the displacement and also the shape and complexity of the signal can vary much [15]. For example, typical displacements from forced breathing is about 20 to 40 mm, while normal breathing gives displacements of about 2 to 4 mm [16]. In contrast, the heartbeat displacement of the chest has a more complex nature since different parts of the heart contracts during different phases of the heartbeat cycle [17]. This results in a more complicated displacement signal, but still, it is possible to see an overall periodicity in the signal. The rate is typically from 60 to 100 beats per minute (BPM) at rest, corresponding to frequencies between 1 and 1.67 Hz [14]. The amplitude of the chest displacements due to heartbeats are much smaller, compared to breathing; typical values are 0.035 to 1 mm [18]. Further, heartbeats also produce heart sounds. In [9], it is shown that these also can be seen as vibrations of the chest wall and measured by a radar. However, heart sounds are expected to be found in a higher frequency range, between 16 to 80 Hz [9]. In each cardiac cycle, there are two primary sounds, as a result of closing valves.

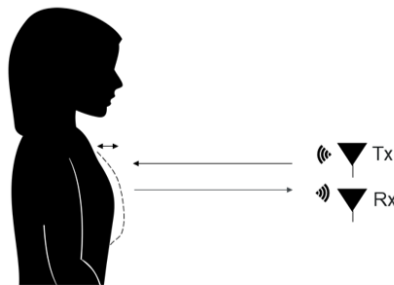


Figure 2.3: Visualisation of vital sign monitoring using a radar.

2.2.1 Reflection and Penetration Depth

Electromagnetic waves that crosses a border between two different media, with different relative permittivity, will be partly transmitted and partly reflected [19]. Different media, such as skin or clothing, have different relative permittivity, and

therefore they will reflect a different fraction of the wave. For example, fabric has a very low relative permittivity and hence also a low level of reflection, which makes measurements through clothing possible, in theory. At 77 GHz the relative permittivity of skin is about 7 [19], and for fabric it is 2 [20]. This corresponds to reflection of 20 % of a wave at the skin surface, and 3 % at the fabric [21]. Also, the 77 GHz signal is rapidly attenuated in the skin due to its lossy characteristics [19]. The penetration depth in skin is below 1 mm, which should be compared to the thickness of the skin, which is about 1.3 – 2.9 mm [19]. Thus, the wave reflected at the chest wall surface will be the most prominent part of the total reflected signal.

2.3 Signal Processing of Radar Signal

The radar signal can be processed in various ways to obtain information of interest. Focus in this section is to describe how phase changes due to small movements of an object can be demodulated from a modulated radar signal. Then follows a theoretical view on wavelet analysis and moving average filtering, which are signal processing techniques explored in this project.

2.3.1 Demodulation Techniques

The output data from the radar is complex valued and needs to be further processed to obtain the desired information. The complex valued data have two components, the in-phase (I) component and the quadrature (Q) component. This type of data is called I/Q data where the I component is the real part and the Q component is the imaginary part of the complex valued data. The process of extracting the phase information from the I/Q data is called demodulation. In the following sections two different demodulation techniques are described.

2.3.1.1 Classic Demodulation

The most common technique for demodulation is called classic demodulation. The process is summarised in Figure 2.4.

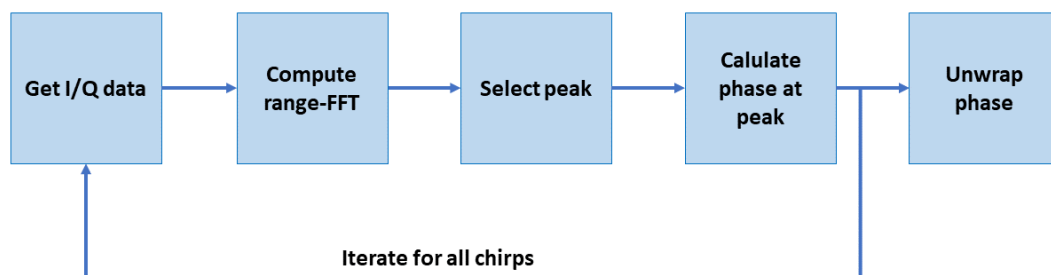


Figure 2.4: The process of classic demodulation

The sampled data from each chirp results in one phase value. Therefore, the phase must be calculated for each segment of data corresponding to one chirp. The first step is to get the I/Q data from one chirp and calculate the Fast Fourier Transform (FFT) of the data. When taking the FFT of the I/Q data the result is a range profile. This particular FFT is called range-FFT since the frequencies on the x-axis can be converted into range, using equation (2.5). The peaks of the range-FFT therefore correspond to reflections from an object at a certain distance. An example can be seen in Figure 2.5. When there is only a single object, it is easy to only consider the largest peak in the range-FFT spectrum. However, when there is more than one large peak, meaning strong reflections from several objects, some strategy for which peak to select must be developed. For the chosen peak, the phase can be calculated as the angle of the complex valued range-FFT output at the peak. The resolution of the range-FFT is the range resolution, equation (2.6), and each point in the range-FFT is usually referred to as a range bin.

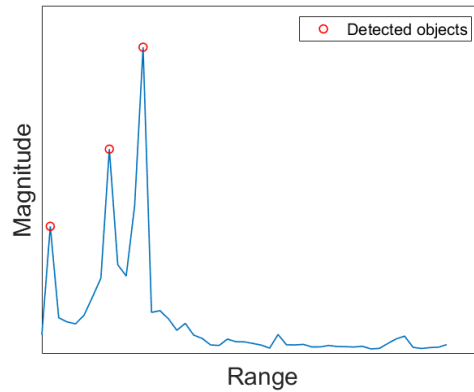


Figure 2.5: Example of a range-FFT with peaks corresponding to objects in front of the radar.

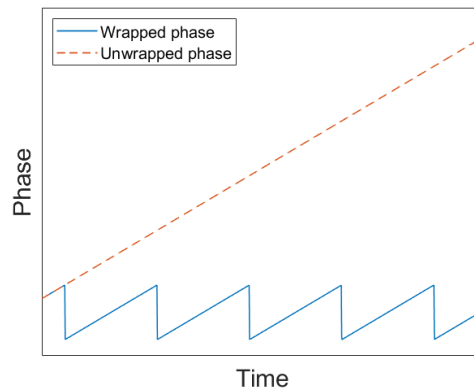


Figure 2.6: Example of wrapped and unwrapped phase.

Iterating this procedure for all chirps produces a phase signal. The phase values are ambiguous due to the fact that they only can take values between $\pm\pi$. The

process of compensating for this is called unwrapping. The most basic unwrapping is to add or subtract a multiple of 2π whenever there is a jump larger than π in the wrapped phase so that the jump become less than π . An example of the wrapping effect and the unwrapped result can be seen in Figure 2.6. After compensating for the wrapping effect, the phase signal can be further processed to obtain relevant information.

2.3.1.2 Linear Demodulation

Another technique used to demodulate the radar signal is linear demodulation. This technique is introduced in [12] as a way to reduce the impact from static reflectors. In short, linear demodulation is based on a principal component analysis, projecting two dimensional I/Q data onto a single dimension [22]. In [22], linear demodulation is described in a few steps. The steps are outlined in Figure 2.7.

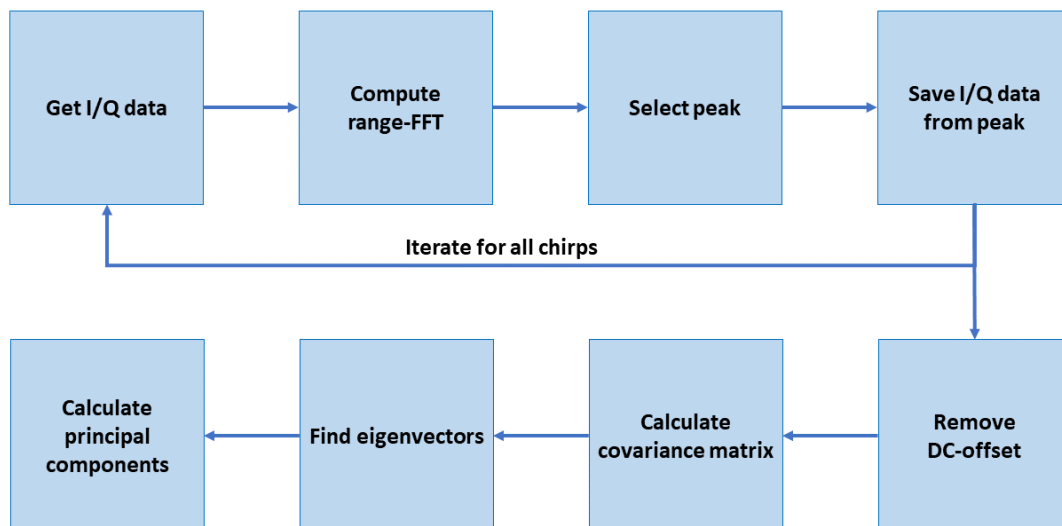


Figure 2.7: The process of linear demodulation

Similar to classic demodulation, a range-FFT is computed based on the I/Q data. For each chirp, the I and Q values at the selected peak are stored in a vector M_{IQ} .

$$M_{IQ} = \begin{bmatrix} I(t) \\ Q(t) \end{bmatrix} \quad (2.9)$$

After iterating through all chirps, the direct current (DC) component in the I and Q channel is removed. This can be done simply by subtracting the average value. A visualisation of this can be seen in Figure 2.8. Further, the principal components of the I and Q data are found. This can be done by calculating the covariance matrix of the I and Q data. Using the covariance matrix, the eigenvalues and eigenvectors

can be found. The principal components of the I/Q data can then be calculated by multiplying the transposed eigenvectors with the I/Q data.

$$X = V^T \cdot M_{IQ} \quad (2.10)$$

where V are the eigenvectors to the covariance matrix, and X are the principal components. The principal component with highest variance can then be taken as the demodulated signal and used for further processing. For example, in Figure 2.8c, the Q component would be taken as the demodulated signal since it has the largest variance.

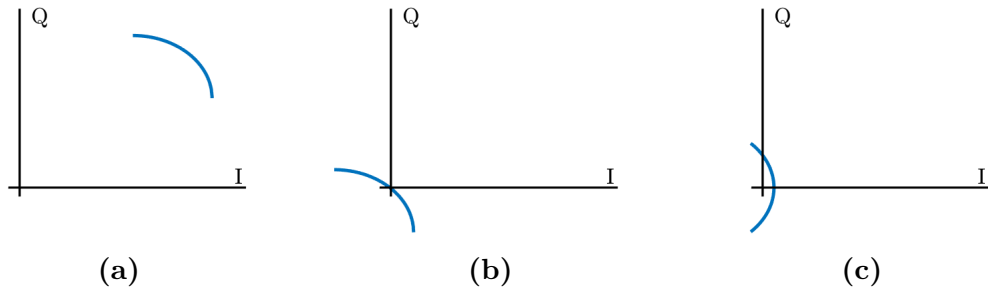


Figure 2.8: Visualisation of linear demodulation. (a) Raw I/Q data. (b) DC component removed. (c) Demodulated data.

2.3.2 Wavelet Analysis

When looking for periodic patterns, such as heartbeats and breathing, it is of interest to analyse the frequencies included in the signal. In the case of physiological signals, we expect that the periodicity will change over time, which means we are also interested in time domain information. Wavelet analysis is a way of extracting both frequency and time information at the same time.

2.3.2.1 Basic Concept

A wavelet is a waveform that is non-zero in a short interval and which mean value is 0 (see an example in Figure 2.9) [23]. Wavelets has two basic properties; *scaling* and *location* [23]. The first one, *scaling*, describes how much the wavelet is stretched, which is related to its frequency content. Second, the *location* property defines the location in time of the wavelet, or in other words the time shift.

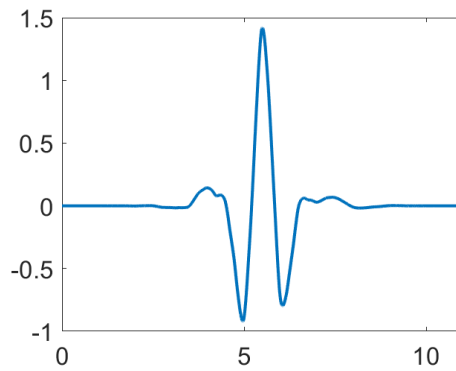


Figure 2.9: Example of a wavelet shape (Symlet 6).

The idea of wavelet analysis is to compare a set of wavelets of different scales with the signal of interest [23]. This is done by convolving the signal with the wavelet for each time step and each scale. There are two main types of wavelet analysis; continuous wavelet transform (CWT) and discrete wavelet transform (DWT) [23]. The basic difference between them is that CWT uses wavelets of all scales, while DWT uses a finite set of scales. The scale of the original wavelet (the mother wavelet) is 1, and, for a specified number of scale levels, the scale is then increasing by a power of 2 for each level.

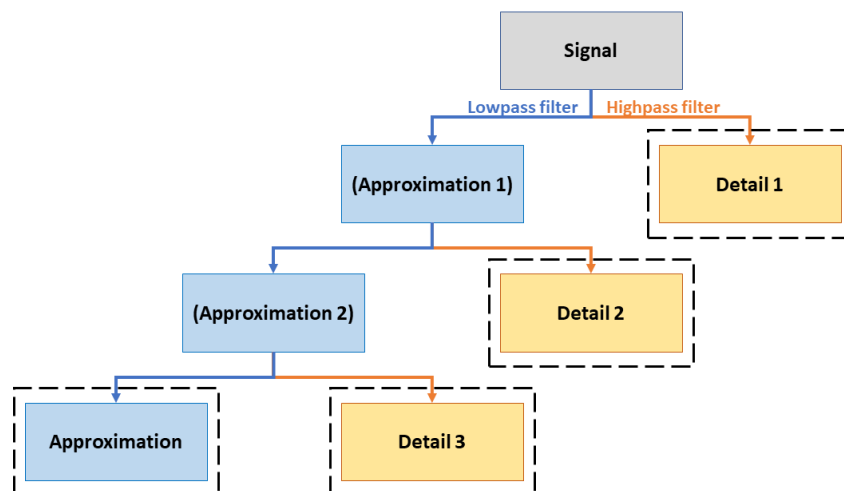


Figure 2.10: Block diagram of wavelet decomposition for DWT. The components included in the final decomposition are marked by dashed lines.

In practice the DWT is performed by applying wavelet decomposition filters to the signal [23], [24]. For each level of decomposition both a high pass and a low pass filter is applied to separate the signal into approximation and details. In the next level the approximation is filtered and separated into a new approximation and details. In the end the decomposition of the signal includes the roughest approximation

coefficients and detail coefficients for all levels. Figure 2.10 shows a block diagram of the decomposition.

The decomposed signal can then be reconstructed back to its original shape by applying the corresponding reconstruction filters [23], [24]. For signal processing purposes the decomposed signal can be modified before reconstruction, in order to enhance interesting behaviours of the signal. This is further described in section 2.3.2.2.

2.3.2.2 Adjustable Parameters for Signal Processing

Signal processing using digital wavelet analysis has some important options and adjustable parameters. This includes the choice of wavelet, how the decomposed data is processed and the number of decomposition levels [23], [24].

To begin with, there are many wavelets with different properties to choose from. When choosing a wavelet, it is important to consider the size, or width, of the non-zero part of the wavelet [24]. This size has to be smaller than the smallest details in the signal. In the case of detecting heartbeats, this means the wavelet cannot be wider than the fastest heartbeat motions. Another important property is the shape of the wavelet. Since the wavelet is convolved with the signal, a wavelet resembling the signal that should be recovered is advantageous.

Second, the processing of the decomposed data has a great impact on the reconstructed signal [23], [24]. For example, certain detail coefficients, or the approximation, can be zeroed out, which means that the reconstructed signal will have no contribution from them. An alternative is to use a threshold value, and zero out everything below that value, but keeping the most prominent parts of the signal.

Also, the level of decomposition is of high importance [23]. When processing the decomposed data, it is of interest to cancel out noise and irrelevant parts of the signal, while saving the relevant parts. This requires the signal to be decomposed to enough levels so that these parts are as separated as possible. Further, the number of levels can be of interest also since it affects the approximation. This matters, for example, if the approximation is zeroed out in order to remove drift in the signal.

2.3.3 Moving Average Filtering

When there is higher frequency noise in a signal, a moving average filter can be used to smooth the signal. The idea is to calculate the average value in a window of the signal, and then slide this window throughout the whole signal. In this way every value in the signal is replaced by the average of its neighbours. Note that this is a sort of low pass filter since the higher frequency content is attenuated when the signal is averaged. The length of the window used decides how much the signal is smoothed, and therefore also how much of the higher frequencies that are removed.

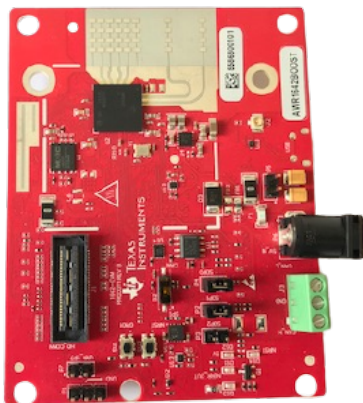
3

Methods

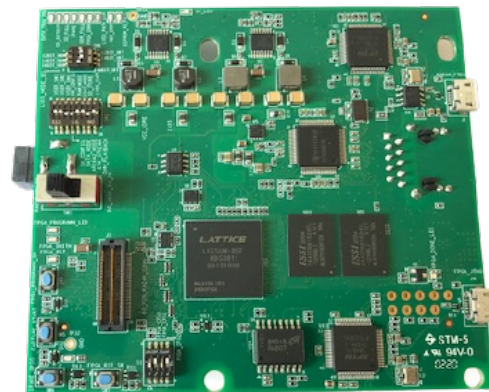
This chapter describe how the project has been carried out. Starting with a detailed presentation of the equipment used, followed by a description of the data collections. In addition, the methods used for signal processing and evaluation are presented.

3.1 Equipment

The radar used in this project was the AWR1642BOOST [25] from Texas Instruments, see Figure 3.1a. AWR1642BOOST is an FMCW radar operating at 77 GHz supporting a bandwidth of 4 GHz. In order to capture raw data from the radar, the capture board DCA1000EVM [26], also from Texas Instruments, was used, see Figure 3.1b. Further, software offered by Texas Instruments called mmWave Studio was used to configure radar parameters and save captured data. mmWave Studio was also used for basic analysis of the captured data. Further analysis and signal processing were done offline in Matlab.



(a)



(b)

Figure 3.1: The radar hardware used. (a) Texas Instruments AWR1642BOOST (b) Texas Instruments DCA1000EVM.

For physiological reference measurements the NeXus-10 MKII [27] from Mind Media was used, shown in Figure 3.2. It is a medical classified (CE Class IIa) biofeedback and neurofeedback device. NeXus-10 MKII supports measurements of a wide range of physiological signals simultaneously and in this project it was used to measure a single-lead ECG along with the respiratory activity using a chest band with a tension sensor. Mind Media also provide a software, BioTrace+, that was used for live visualisation and recording of ECG and respiratory activity. Additionally, a camera was used to capture a video stream in BioTrace+, allowing synchronisation, further described in section 3.2.



Figure 3.2: NeXus-10 MKII. Image used with permission [28].

3.1.1 Radar Configuration

As described in theory section 2.1 there are several parameters to consider when configuring the radar. The shape of the chirp, i.e. the start frequency, the bandwidth, and the time duration, affects what can be measured by the radar. It affects for example the range resolution and the penetration depth of the transmitted radar signal. In this project a radar system with a start frequency of 77 GHz was used, resulting in a short penetration depth, about 1 mm [19]. This means that we only measure the movements of the skin of the chest wall and not the movements of inner organs. The time duration of the chirp was set to 20 μ s and a bandwidth of 3.4 GHz was used. Thus, the range resolution was about 4 cm, according to equation (2.6). Further, the received radar signal was sampled by the ADC with the frequency 6.25 MHz. A new chirp was sent out every 40 ms, and since each chirp gives one phase value, this resulted in a sampling frequency of 25 Hz for the phase signal, enough to resolve both heartbeats and breathing.

3.2 Data Collections

During the project, data has been collected in two separate rounds. The data collections have many similarities but also some differences. Below, a general description of the test setup is given, together with details about both of the data collections.

3.2.1 Test Setup

During the data collections data from both the radar and the reference sensors were recorded. The radar data were transferred to a PC via ethernet and the reference data were wirelessly connected via Bluetooth. In order to synchronise the two data streams, a camera was connected to the NeXus-10, reference device. This allows for a video stream with the same time frame as the reference measurements. An event visible both in the radar signal and on the video allow the two data sources to be manually synchronised afterwards.

The collection of data was carried on a vibration rig, simulating the vibrations in a car. The main reason for conducting the tests in a rig was to avoid safety issues related to driving a real car in traffic, but also to increase the repeatability of the tests. The vibration rig takes vibration data as input and based on that it vibrates in three axes. On top of the vibrating platform a seat with associated belt and a steering wheel was mounted. The test setup can be seen in Figure 3.3.



Figure 3.3: Test setup with driver seat and steering wheel mounted on a vibrating rig.

As mentioned, the rig vibrates in three axes, x , y and z . Before the setup of the rig, vibration data from real driving were recorded. The recordings used are based on acceleration data collected during driving. The recorded accelerations were then recalculated into x - y and z displacements in order to fit the input to the vibration rig. Also, since the recorded vibrations were sampled at 6000 Hz and the vibration rig only support up to 200 Hz, a down sampling had to be done. For the results of this project, a vibration profile recorded on the highway at around 110 km/h was used.

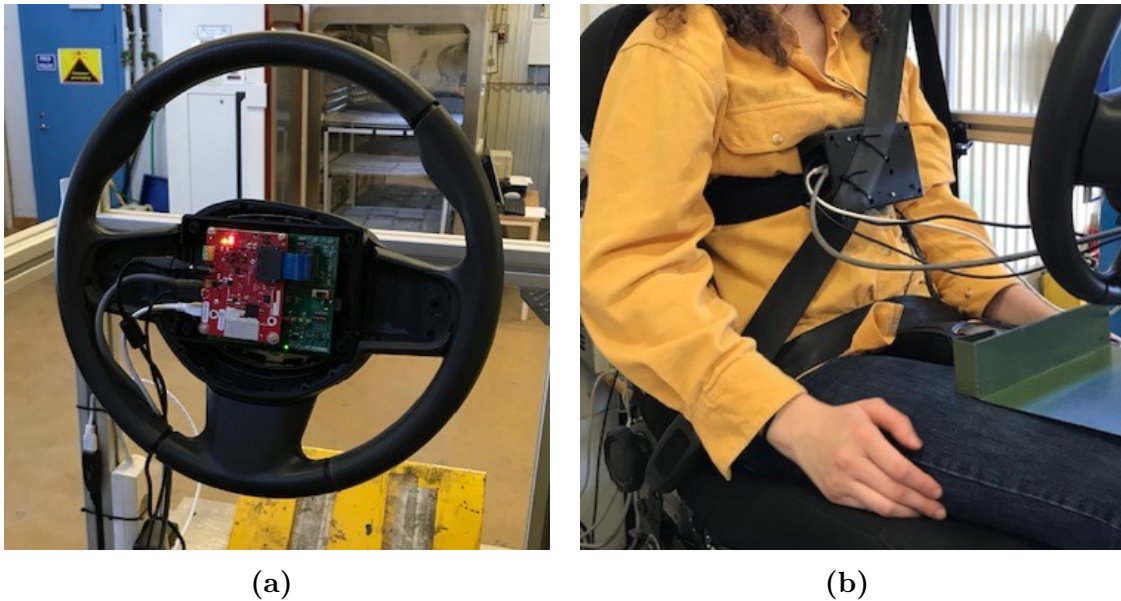


Figure 3.4: Antenna locations during data collection; steering wheel (a) and seat belt (b).

For the antenna location two different cases were used; mounted on the steering wheel and on the seat belt, see Figure 3.4. For the first case the steering wheel was kept fixed, in order to simplify the signal processing for this initial testing case. The radar was attached to the steering wheel and aimed toward the subject's chest, in order to detect the vibrations of the chest wall. For the second case, the seat belt, the radar was covered by a plastic box, in order to protect the electronics. This means we have to consider that the air gap, of about 2 cm, between the radar sensor and the body is slightly larger than if the sensor was integrated in the seat belt. Also, reflections from the cover could possibly interfere with the chest wall signal. However, the cover will always have approximately the same distance to the radar, which means it will only contribute with a DC component. Further, the air gap between the sensor and the body is important to at all get a useful signal, but it does not need to be as large as the gap caused by the cover. This was tried by making some careful measurements where the sensor was gently placed on the chest without the cover, and it turned out that the air gap from the clothing was enough. Another issue with the seat belt position is that the radar equipment is relatively heavy, which means it is hard to make a stable experimental setup. To prevent the seat belt from hanging, due to the heavy equipment, it was set to have a fixed length. This made the setup more stable.

3.2.2 Data Collection 1

For the first data collection several different variables were varied and tested. Particularly, the antenna location was varied, two types of vibrations were used, different clothing were tested and the amount of movements from the test subject was changed. For the movements a sequence of different movements was used. The

movements included steering movements and adjusting the positioning, but also talking. These events were seen as a regular part of driving and would therefore be interesting to investigate. The movement sequence as a whole can be seen in Appendix A. In total, 24 different test cases were conducted, each with a length of 5 minutes. A summary of the tests can be seen in Appendix A .

3.2.3 Data Collection 2

After the first data collection it was decided to focus on the seat belt position, due to time limitations of the project. It is reasonable to think that the signals from the steering wheel and the seat belt will have slightly different characteristics and therefore could benefit from different signal processing approaches. Also, since the steering wheel case has the simplification with the fixed steering wheel, the seat belt position was considered a more realistic case and therefore also more relevant. Therefore, in the second data collection, measurements from the seat belt position was further investigated. Also, the reason to do this second collection was to collect more data from each test case, to get a better overview of what the data looks like in general. Thus, there were more measurements of the same cases, and fewer parameters considered during each case. From the basic case, without vibrations and sitting still, some parameters were varied. For example, motorway vibrations, talking and small steering movements were added, one at the time. In total there were 24 test cases, of 4 minutes each. See Appendix A for a summary of the tests.

The second data collection also included tests to investigate the feasibility of detecting heart sounds. For these tests, no vibrations were used, the subject was sitting still and wore normal clothing. According to [9], heart sounds can be found in the frequency range 16-80 Hz, therefore an increased sampling frequency was used for these tests.

3.3 Data Processing and Analysis

The signal processing of the radar signal can be divided into some overall steps, with a few smaller differences between breathing and heartbeat detection, which will be further described below. Figure 3.5 shows these steps in a block diagram. In the first step, the phase signal is demodulated from the radar data, as described in section 2.3.1. Here, also a relevant range bin is chosen. Second, the phase signal has some baseline drift that is removed to facilitate further signal processing. Then, the signal is filtered further to recover the signal of interest; heartbeats or breathing. From these filtered signals, the heartbeats and breathing events can then be found by peak detection, and using these peaks the inter beat interval (IBI), and inter breath interval (IBI), can be calculated. Further, the IBIs can be used to calculate the average HR and BR, by taking the average of the IBI in time windows. Finally, the HR and BR is compared with the reference measurements to calculate an accuracy measure. Moreover, the reference signals need some simpler signal processing, in terms of baseline drift removal and peak detection, which will be described in section 3.3.5.

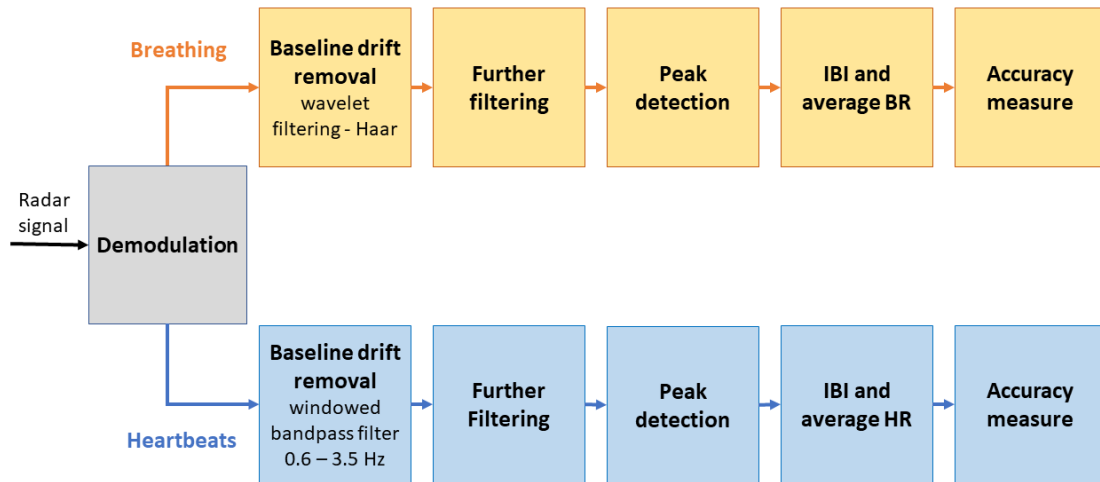


Figure 3.5: Block diagram of the general steps of the signal processing.

3.3.1 Demodulation and Range Bin Selection

The phase is extracted from the radar signal, as described in section 2.3.1. Classic demodulation is used as default, but also the linear demodulation has been evaluated. However, one of the challenges is how to choose range bin over time. As mentioned in section 3.1.1, the range resolution in our case is about 4 cm. Even though the driver does not sit completely still, the movements are assumed to be within two neighbouring range bins.

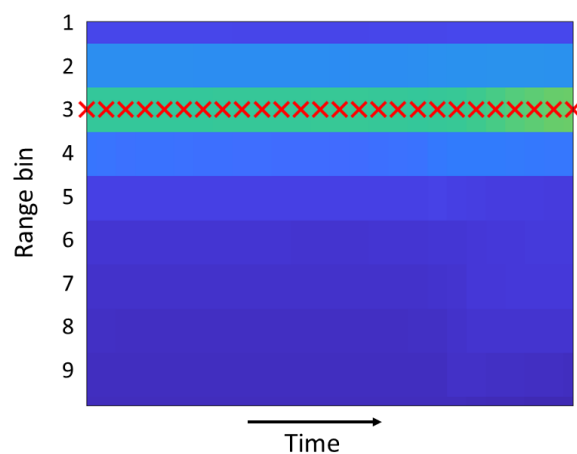


Figure 3.6: Example of range bin selection, red cross representing a detection.

The strategy for choosing range bin is based on the magnitude of the range-FFT. For each emitted chirp, the peak corresponding to the maximum reflection is identified and considered a detection. The range bin number of this detection is then saved. Counting the number of detections in each range bin allow selection of the range bin with most detections. Further, the neighbouring range bins are investigated. If 20% or more of the total number of detections are in any of the neighbouring range bins, then both range bins are considered relevant. In that case the phase signals for both range bins are calculated and combined into an average phase signal. Otherwise, only the range bin with most detections is selected. To further describe the concept, an example is shown in Figure 3.6. Here all detections are in range bin three, and hence this range bin would be selected.

3.3.2 Baseline Drift Removal

As mentioned, the data often has a baseline drift that has to be removed. This facilitates, for example, peak detection later on. See an example of a signal before and after baseline drift removal, in Figure 3.7. The method for removing the baseline drift is different for the breathing and the heartbeat extraction cases.

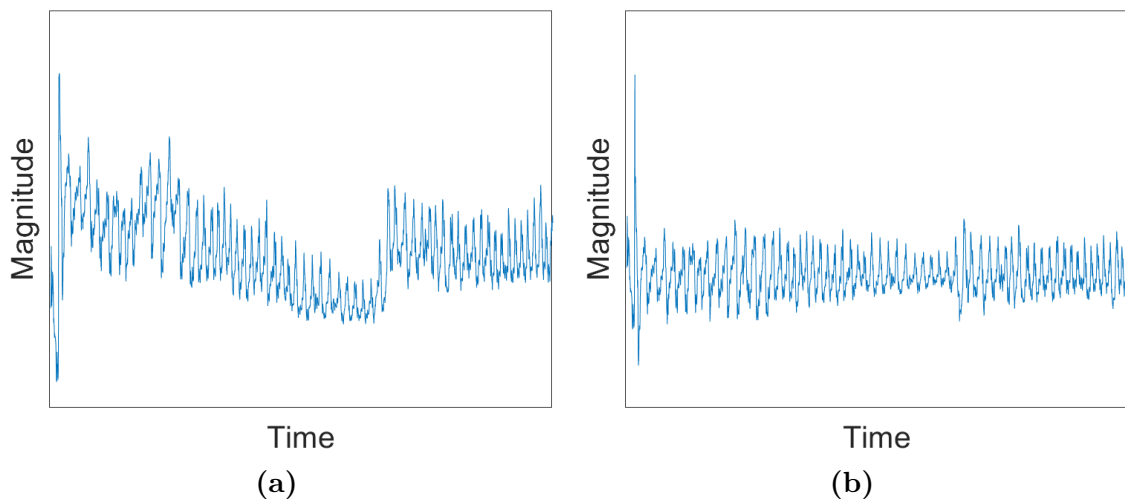


Figure 3.7: Example of signal with baseline drift (a) and after removal (b) using the wavelet approach.

For the heartbeats, a windowed band pass filter is applied. It uses the Hamming window and the passband is 0.6 - 3.5 Hz, which corresponds to 36 - 210 BPM. Heartbeat patterns should be in that range [14]. Here, the lower cut-off frequency is set quite low, to avoid removing important signal information for lower HR. However, since the baseline drift mostly consists of low frequent signal content, the band pass filter will remove the drift. Furthermore, the band pass filter will also function as a first step in extracting the heartbeat information, since frequencies outside the range of interest will be attenuated.

Breathing, on the other hand, can include very low frequencies, and therefore, a band

pass or high pass filter is not a suitable option, since it also risks removing important content of the breathing signal. Instead wavelet analysis is used, utilising that if the signal is decomposed long enough, the approximation coefficients correspond to the baseline drift. These approximation coefficients can then be zeroed in order to remove the baseline drift. Here, the Haar wavelet is used. That is a box shaped wavelet, which is especially good at estimating sharp jumps. This turns out to be a useful property since, in addition to the baseline drift, there also often appear sharp changes in the signal, due to movements. Using the Haar wavelet can therefore also approximate these artifacts.

3.3.3 Filtering to Extract Heartbeats and Breathing

For the extraction of heartbeats and breathing, some different methods has been tried out. Mainly, a method using wavelets, and a moving average based approach, has been investigated, both separate and in combination. A summary of the parameters used to extract breathing and heartbeats is shown in Table 3.1.

In previous research, wavelets have been used successfully to separate breathing and heartbeats, but also to remove noise [8], [12]. The wavelet based method in this thesis uses the concept described in section 2.3.2.2, where the signal is wavelet decomposed and certain detail coefficients of interest are kept, while the others are zeroed out. For the breathing extraction, the Coiflet 2 wavelet is used. The signal is decomposed to level 4 and the approximation is saved, while all detail coefficients are zeroed out. Heartbeats extraction instead, uses the Biorthogonal 6.8 wavelet and decomposes to level 7. The approximation, together with detail coefficients 3, 4 and 5 are kept, while the remaining details are zeroed out.

By only using the wavelet based method, there were problems with overdetection of peaks. Therefore, a moving average filter was added, in order to get rid of smaller, false peaks. The moving average filtering uses the Matlab function `movmean`, which applies a moving average filter with a specified length on the signal. Based on an investigation of different lengths, the length is set to 25 samples for breathing, and 10 samples for heartbeats. After the moving average filters were tried out together with the wavelets, we also investigated the performance of the moving average filters alone. This resulted in similar performance, and in the end only the moving average filter was used as the standard method.

Table 3.1: Signal processing parameters.

	Wavelet	Decomposition level	Coefficients used	Moving average length (samples)
BR extraction	Coiflet 2	4	approx. 4	25
HR extraction	Bior 6.8	7	det. 3,4,5	10

3.3.4 Peak Detection and Average Heart Rate and Breathing Rate Calculations

After filtering out the heartbeat and breathing patterns from the data, it is of interest to localise the peaks corresponding to the heartbeats and breathing events. For this a peak detection method has been developed. It uses the Matlab function `findpeaks`, which finds the height and location of the peaks in the input data. It has the option to specify some parameters deciding what counts as a peak, for example, the minimal distance between two peaks and the minimum prominence. The latter is a measure of the height of the peaks in comparison to surrounding valleys. In the developed peak detection method this prominence is set as a fraction of the root mean square (RMS) value of the signal. To make the peak detection more adaptive and less sensitive to changes of signal strength, a sliding window approach is used. In each window the minimum prominence is updated with the RMS-value in the current window before the peaks are found. To be sure not to miss peaks near the edge of a window, all windows overlap half of the window before. Afterwards, double detected peaks and peaks located too close to each other are removed. For both heartbeats and breathing, the windows used for peak detection are 10s and the prominence is set to 0.3 times the RMS-value, based on empirical studies.

Also, the minimum peak distance is specified for this method. For the heartbeats it is set to 0.4s, which corresponds to a HR of 150 BPM. Higher HR was not considered relevant in this situation. For breathing, instead, this distance is 1.2s, corresponding to 50 BPM, which is higher than for normal breathing, but since the breathing is also partly controlled by the person, some shorter breaths can occur even though the overall BR is slower.

After the peaks are found, the IBI can be calculated as the distance between all neighbouring peaks. The IBI can then, in turn, be used to calculate the average HR and BR. This is done by taking the average IBI in sliding time windows and converting it to beats or breaths per minute. For these average calculations, the windows are 20s for breathing and 10s for heartbeats, and moved by 5s at the time, so that they overlap.

3.3.5 Signal Processing of the Reference Data

The reference signals are not subject to any advanced signal processing. However, there is some baseline drifts that complicates the procedure of finding peaks. Therefore, the baseline drift is removed in both reference signals. The drift is removed using the same technique as for the breathing, described in section 3.3.2. Here, the Symlet 7 wavelet is used for decomposition to level 9 and 12, for heartbeats and breathing respectively.

To enable a comparison of the radar signals and the reference it is of interest to find the peaks. For the peak detection in the breathing reference the same method as described in section 3.3.4 is used. For the heartbeat reference the Matlab function

`findpeaks` is applied to the whole signal, without using a window, since the peaks are very prominent. Here, the minimum distance between the peaks is set to 0.4 s and the minimum peak prominence is set to 50 % of the range that the signal span.

Further, the average BR and HR are calculated using the method described in 3.3.4, where the average IBI is calculated in a time window. The window lengths are 20 and 10 s, for BR and HR, respectively.

3.3.6 Evaluation

In early stages, the performance of the signal processing was evaluated subjectively by a visual comparison with the reference signals. However, a more objective evaluation was needed. An accuracy measurement used in [29] was adopted and both the mean and median accuracy were used as a quantitative measurement of the performance. The mean, having the benefit of indicating the overall performance. On the other hand, the median is more robust to outliers, making both of them valuable measurements of the performance. The accuracy is calculated as

$$Accuracy = \frac{R_{ref} - |R_{ref} - R_{radar}|}{R_{ref}} \times 100 \quad (3.1)$$

where R_{ref} or R_{radar} are the average BR and HR in a window. For breathing, a 20 s window is used and 10 s for heartbeats. Note that the accuracy is a relative measurement. This means that a 1 % error in the average rate will be different in absolute values for different measurements. In general, since the BR is lower, an absolute error of 1 BPM for the BR will give a lower accuracy than an absolute error of 1 BPM for the HR. That should be kept in mind when evaluating the performance.

3.4 Heart Sound Detection

As mentioned, in this project we also investigate the possibility of measuring heart sounds using radar. For this a higher sampling frequency, 200 Hz, is used. In order to extract heart sounds the signal is band pass filtered between 16 and 80 Hz, which is the relevant frequency range for heart sounds.

To get an idea of the feasibility of this method, the heart sound signal is briefly investigated. The peaks of the first heart sound in each cardiac cycle is manually annotated, and the IBI is calculated. This is then compared to the IBI of the reference and the accuracy is calculated according to section 3.3.6.

4

Results

This chapter deals with the results of this project. It begins by displaying results concerning the effect of parameters such as body movements, talking and vibrations. Unless anything else is specified, the signal processing used to produce the results in this chapter are based on the moving average filtering outlined in section 3.3, together with the classic demodulation technique. With that being said, interesting results obtained by using different signal processing methods are highlighted in section 4.2. As mentioned before, only results regarding measurements from the seat belt are presented. However, in section 4.3 we take a short look at the data from the steering wheel, together with initial results related to heart sounds.

4.1 Results for Different Test Conditions

There are several parameters that have been varied during the data collections. In this section, results related to the most important ones are presented. This include results from the simplest case with a stationary test subject, with added vibrations, talking, body movements and also a short look at the impact of thicker clothing.

4.1.1 Stationary Test Subject

The most trivial case tested are the ones without vibrations and where the subject is instructed to sit still in the driving seat, with their hands on the steering wheel. The average BR and HR for two such measurements are shown in Figure 4.1. From Figure 4.1 we can see that, for the majority of the time the average BR and HR follows the reference. However, both for the average BR and average HR, there are sections where the measured rates deviate from the reference. Worth pointing out is that the test cases shown in Figure 4.1, involve two different test subjects.

4. Results

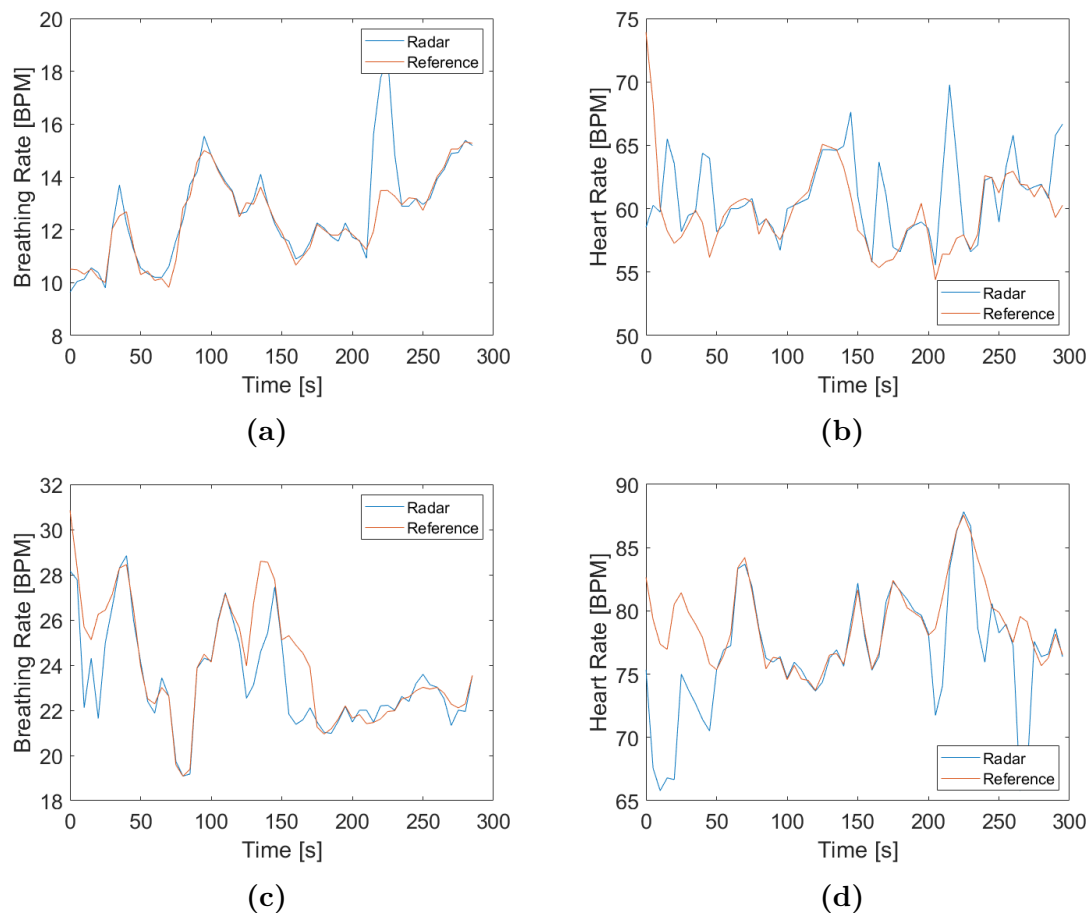


Figure 4.1: Average BR ((a) and (c)) and HR ((b) and (d)) for two test cases where the test subjects are sitting still. (a) and (b) are from the same test, and the same applies for (c) and (d).

During data collection two, several measurements for the same test case were done. In Figure 4.2 the demodulated radar signal for four different measurements, of the same test subject, are shown. Figure 4.2 show clear differences between the demodulated signals, even though they are measured for the same test case and on the same subject. Since the signals have such different shapes, the resulting BR and HR calculations also differ. The mean and median accuracy for both average BR and average HR were calculated for all four measurements. A summary are presented in Table 4.1. Note that for the signal shown in Figure 4.2a, the accuracy are significantly lower for both BR and HR, whereas the other three result in similar accuracies.

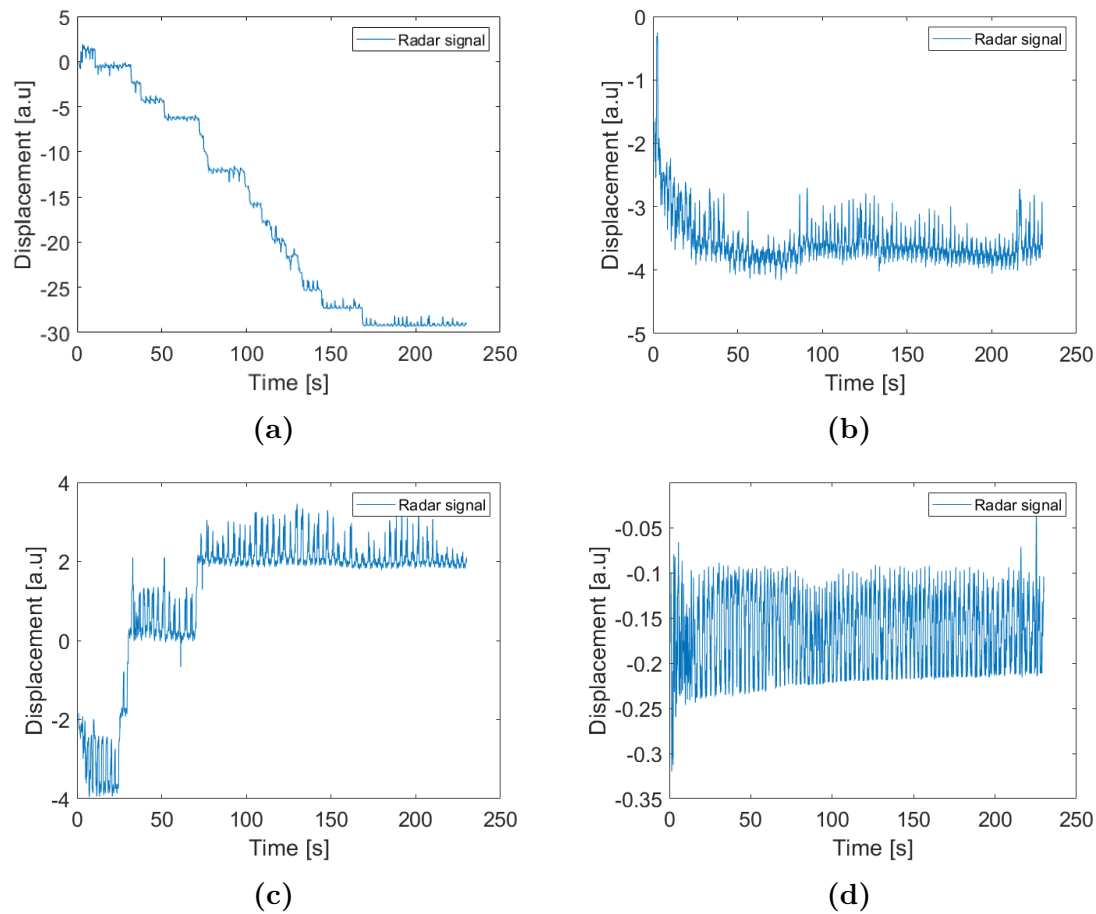


Figure 4.2: Demodulated radar signal for four different measurements with the same test conditions and subject. The test condition is without vibrations and movements.

Table 4.1: Summary of accuracy of signals shown in Figure 4.2.

Figure	BR Accuracy (%)		HR Accuracy (%)	
	mean	median	mean	median
(a)	90.8	91.7	84.8	85.2
(b)	94.6	98.8	98.7	99.5
(c)	95.9	98.5	97.0	99.1
(d)	96.7	99.0	95.6	98.2

In total 11 measurements where the test subject sits still were conducted. The mean and median accuracy for all of them can be seen in Table 4.2. In order to get an indication of the general performance for the case without vibrations and movements, the average of each accuracy measurement is presented in the last row. We see that the average of the mean BR accuracy is 92.9% and the average of the mean HR accuracy is 91.2%. In contrast, the highest mean accuracies achieved are 96.8% for BR and 98.7% for HR. Assuming a BR between 10-30 BPM this

corresponds to an error of about 0.3-1 BPM. For HR the same calculation gives an error of about 0.8-1 BPM, given a HR between 60-80 BPM.

Table 4.2: Summary of accuracy for BR and HR when test subject sit still.

BR Accuracy (%)		HR Accuracy (%)		
mean	median	mean	median	
96.3	98.5	96.2	99.1	
96.8	98.9	96.8	99.4	
75.5	97.1	98.0	99.3	
94.5	98.1	81.5	84.0	
92.5	96.9	82.6	87.9	
90.8	91.7	84.8	85.2	
94.6	98.8	98.7	99.5	
95.9	98.5	97.0	99.1	
96.5	97.9	73.9	72.3	
96.7	99.0	95.6	98.2	
91.9	98.4	98.1	99.4	
Average:	92.9	97.6	91.2	93.0

4.1.2 Impact of Steering Movements

One of the major challenges with extracting vital signs from chest vibrations is body movements. In Figure 4.3, part of a measured signal is shown, demonstrating the impact of small steering movements. The test subject is instructed to simulate motorway driving, with small corrective steering movements. In Figure 4.3a, the test subject sits still until around 100 seconds where the small steering movements start. It can be seen that even small movements have a strong impact on the measured signal. This is also seen in the average BR shown in Figure 4.3b, where it follows the reference up until 80s. Since the window used to calculate the average BR is 20s seconds long, this correspond to the start time for the steering movements.

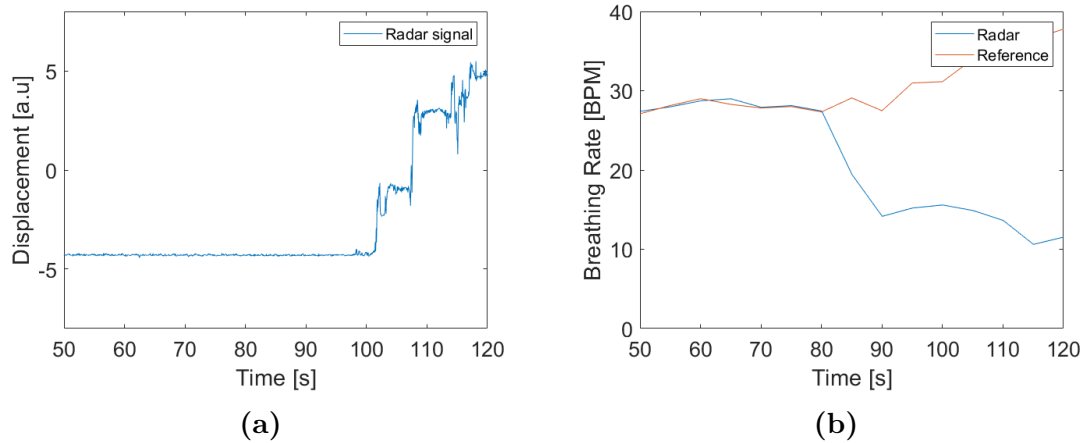


Figure 4.3: Demodulated radar signal (a) and average BR (b) when test subject start small steering movements.

The second data collection included several measurements where the test subject performed small steering movements for the whole test. Examples of the demodulated signal for these measurements are presented in Figure 4.4. Looking at the signals in Figure 4.4, it can be seen that the small steering movements cause large distortions. Compared to the signals in Figure 4.2, where the test subject sit still, the signals in Figure 4.4 are quite different and more irregular. The irregularity of the signals also affects the estimated accuracy for BR and HR. In Figure 4.5 the average BR and HR for the signal shown in Figure 4.4a are presented. The corresponding mean accuracies are 81.7% for BR and 89.4% for HR.

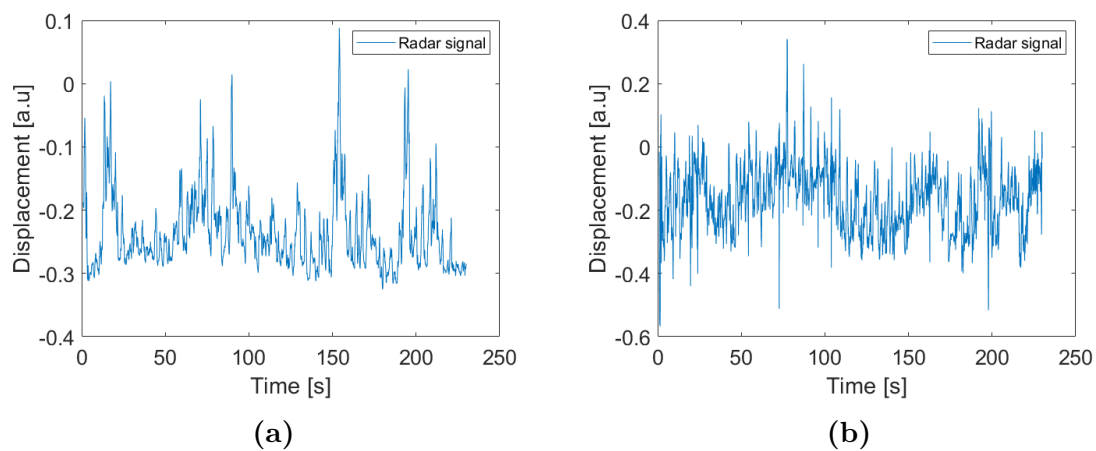


Figure 4.4: Demodulated radar signal from two different tests with steering movements.

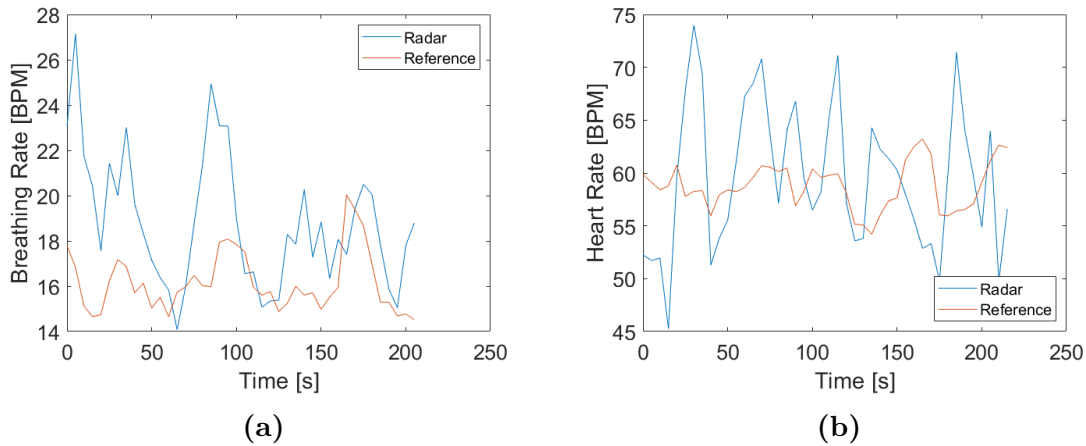


Figure 4.5: Average BR (a) and HR (b) for the signal shown in Figure 4.4a.

In total, four measurements were conducted when the test subjects performed small steering movements for the whole test. The accuracies for these measurements are presented in Table 4.3. Comparing the average accuracy results in Table 4.3 with those in Table 4.2, we see that the average BR accuracy is lower with movements. This effect is not seen when comparing the average HR accuracies.

Table 4.3: Summary of accuracy for measurements with small steering movements from the test subject, during the whole test.

BR Accuracy (%)		HR Accuracy (%)		
mean	median	mean	median	
70.1	73.5	91.3	93.6	
81.7	86.1	89.4	90.6	
83.7	87.3	92.0	93.4	
86.8	88.5	92.3	95.5	
Average:	80.6	83.9	91.3	93.3

4.1.3 Performance with Vibrations

As described earlier, the tests were conducted on a vibration rig using vibration data collected during real driving. In this section, the effect of vibrations will be presented. In Figure 4.6 examples of demodulated radar signals measured with motorway vibrations are shown. The signals presented in Figure 4.6 are from two measurements of two different test subjects. Both of the signals are somewhat affected by the vibrations. As mentioned in section 4.1.1, there are significant differences in the signal between different measurements of the same test case.

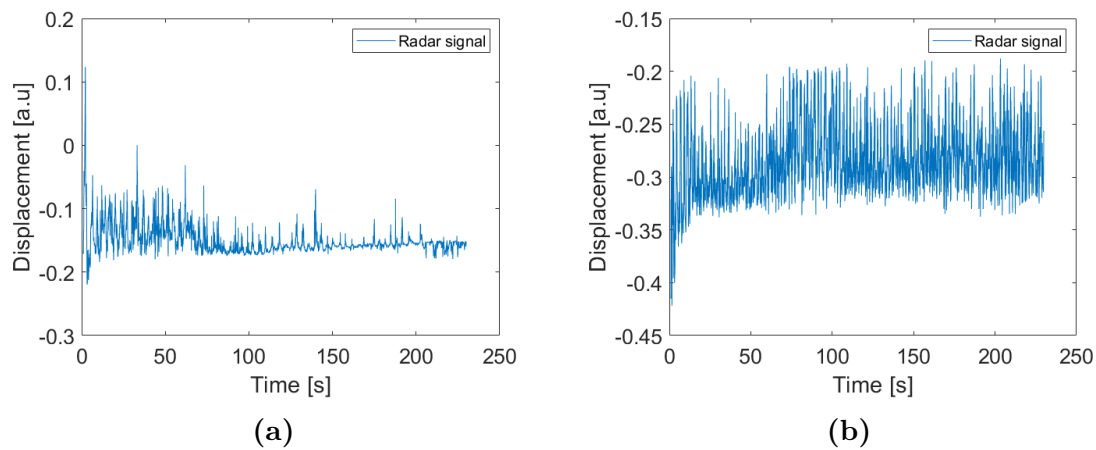


Figure 4.6: Examples of demodulated radar signals from measurements with motorway vibrations.

In addition, the average BR for the cases in Figure 4.6 are calculated and presented in Figure 4.7. Notice that in Figure 4.7b the average BR follows the reference, but in Figure 4.7a, there are several parts where the measured average BR deviates from the reference. The accuracy for the average BR shown in Figure 4.7a is 83.8% in mean and 83.2% in median, while the accuracy in Figure 4.7b is 98.9% in mean and 99.0% in median.

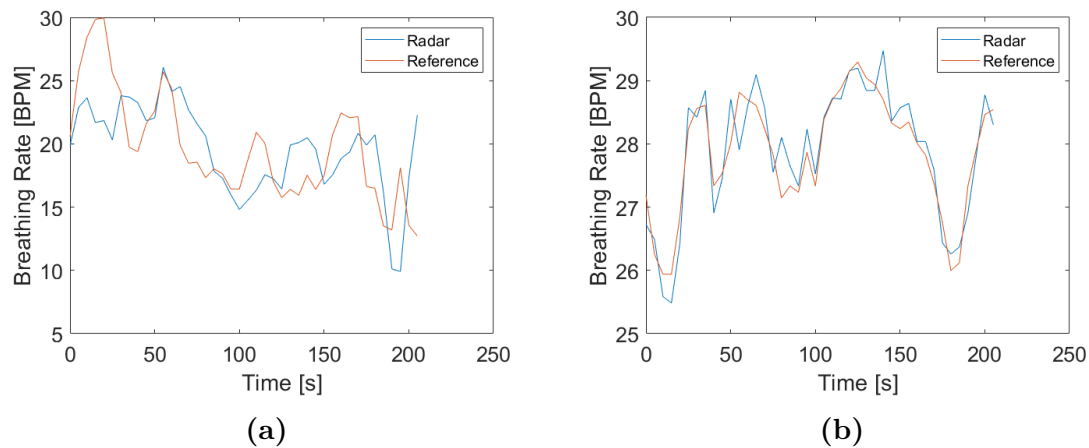


Figure 4.7: Average BR for the signal in Figure 4.6a in (a) and for the signal in Figure 4.6b in (b).

In total, there was nine measurements while the test subjects sat still, and motorway vibrations were applied. The resulting accuracies for both average BR and average HR are presented in Table 4.4. We can see a great variance in accuracy between the measurements, for example the mean accuracy for BR, ranging from 62.7% to 98.9%. Further, comparing to the average accuracies without vibrations, seen in Table 4.2, the average accuracies with vibrations are lower.

Table 4.4: Summary of accuracy for measurements with motorway vibrations.

	BR Accuracy (%)		HR Accuracy (%)	
	mean	median	mean	median
	82.3	93.9	87.3	88.0
	92.6	98.2	90.4	91.6
	83.8	83.2	85.2	86.0
	87.4	93.7	83.5	84.9
	91.1	97.4	86.2	87.6
	62.7	73.2	89.7	90.5
	97.7	98.9	97.5	98.8
	98.9	99.0	95.6	98.2
	91.5	92.2	92.1	93.3
Average:	87.6	92.2	89.7	91.0

4.1.4 Effects of Talking

Talking affects the subject's breathing pattern, and hence, also the signal that can be measured. Figure 4.8 shows an example where the subject breathes normally at the beginning and then says the days of the week in a calm pace. Disruption in the breathing pattern can be observed in both the radar and the reference signal. Also, note that in the reference data the breathing is still clearly seen, while in the radar signal the breathing pattern is not clear.

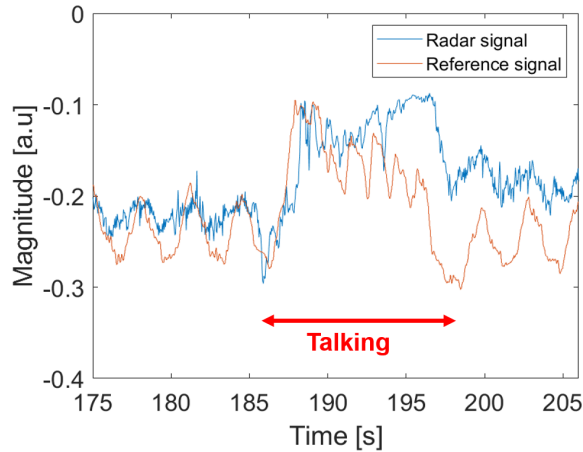


Figure 4.8: The effects of talking. Here, the breathing pattern is disrupted when the subject says the days of the week in a calm pace.

Further, some measurements were performed when the subject had a conversation during the measurement. In Figure 4.9 the average BR for one of those cases is shown. Note that for both the radar and the reference, the estimated rate fluctuates much between higher and lower rates. Also, worth to mention is that the radar follows the general trend in the reference to some extent. In this particular case the mean and median accuracies are 78.6% and 80.2%, respectively. In Table 4.5

the accuracies for all measurements during a conversation are presented. Here, also accuracies for the estimated HR for the same cases are shown. Worth to remember is that the accuracy is given in percentage of the BPM value, which means that the accuracies for HR and BR should not be directly compared to each other. In this case, an accuracy of about 70 % for the BR means an error of 3-9 BPM if we consider BR between 10 and 30 BPM. Similarly, for HR an accuracy of about 90 % corresponds to 6-8 BPM error, assuming a HR between 60 and 80 BPM.

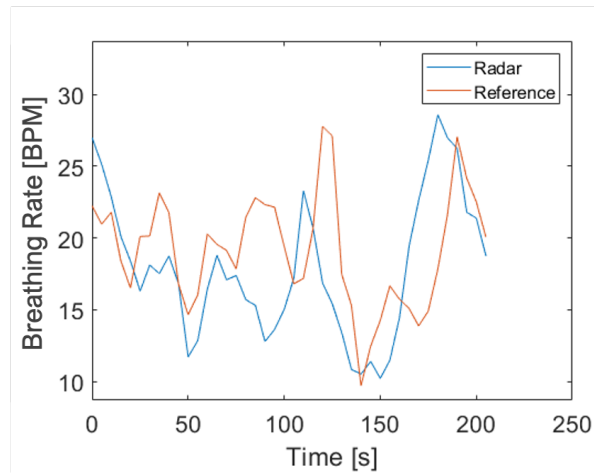


Figure 4.9: Average BR for a measurement when the subject had a conversation during the complete measurement.

Table 4.5: Summary of accuracy for measurements during a conversation.

BR Accuracy (%)		HR Accuracy (%)	
mean	median	mean	median
75.0	85.5	91.3	92.7
78.6	80.2	88.6	89.9
59.0	63.2	92.8	94.5
48.9	67.2	90.4	93.1
Average: 65.4	74.0	90.8	92.6

4.1.5 Measurements Wearing a Jacket

In the first data collection set, also two measurements, where the subject wore a jacket, were conducted. These cases also had vibrations applied and the subject did movements according to a predefined sequence. At two times in the sequence, the task was to sit still during a longer time period. Figure 4.10 shows an example of the average BR and HR from one of these stationary parts. For this case the BR accuracies are 96.3 % and 97.4 % in mean and median, respectively, and for the HR the mean and median accuracies are 95.2 % and 98.2 %. In Table 4.6 the accuracies for all four parts are presented. Note that the case shown in Figure 4.10 has the highest mean accuracy for both BR and HR.

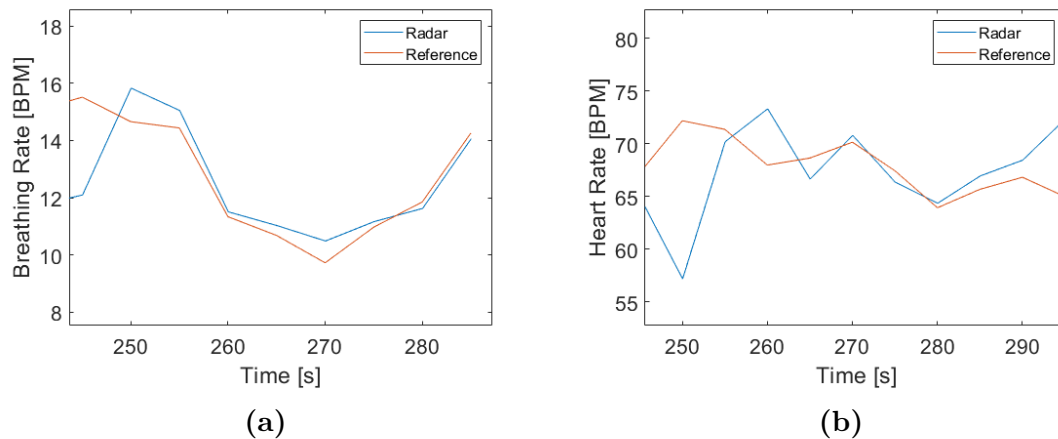


Figure 4.10: (a) Average BR and (b) HR for a case where the subject wore a jacket. Here, also vibrations were applied.

Since the measurements are performed with vibrations applied the results in Table 4.6 should be compared to Table 4.4 which also presents results where there are vibrations applied, but without jacket. The results show that the average accuracies are quite similar for the case with and without jacket.

Table 4.6: Summary of accuracy for measurements with the subject wearing a jacket. For all cases the subject is sitting still, but vibrations are applied.

BR Accuracy (%)		HR Accuracy (%)		
mean	median	mean	median	
83.5	90.0	91.7	91.5	
96.3	97.4	95.2	98.2	
91.2	95.1	83.2	84.4	
93.5	98.8	86.6	85.3	
Average:	91.1	95.3	89.2	89.9

4.2 Results Related to Signal Processing

There are many parameters related to the signal processing methods used during this project. In the following section, a few interesting signal processing aspects are presented, highlighting the difficulty in choosing a general signal processing method.

4.2.1 Comparison of Wavelet Analysis and Moving Average Filtering

The standard method in this project for filtering out the heartbeat and breathing patterns uses the moving average approach described in section 3.3.3. However, also the wavelet based method, described in the same section, was explored as well as a combination of the two.

First, the wavelet based method used alone produced ambiguous results, which is illustrated in Figure 4.11. The figure includes BR and HR from two test cases. In both cases the subject was sitting still and there were no vibrations applied. Further, the measurements are from different test subjects. Note also that the BR and HR range is different for the two cases. Worth to point out is that for the case in Figure 4.11c and 4.11d the estimated BR and HR follows the reference to high extent, while in Figure 4.11a and 4.11b there are more deviation, mostly in terms of too high rates, which corresponds to too many detected peaks. This difference between the cases is also reflected in the accuracy values presented in Table 4.7.

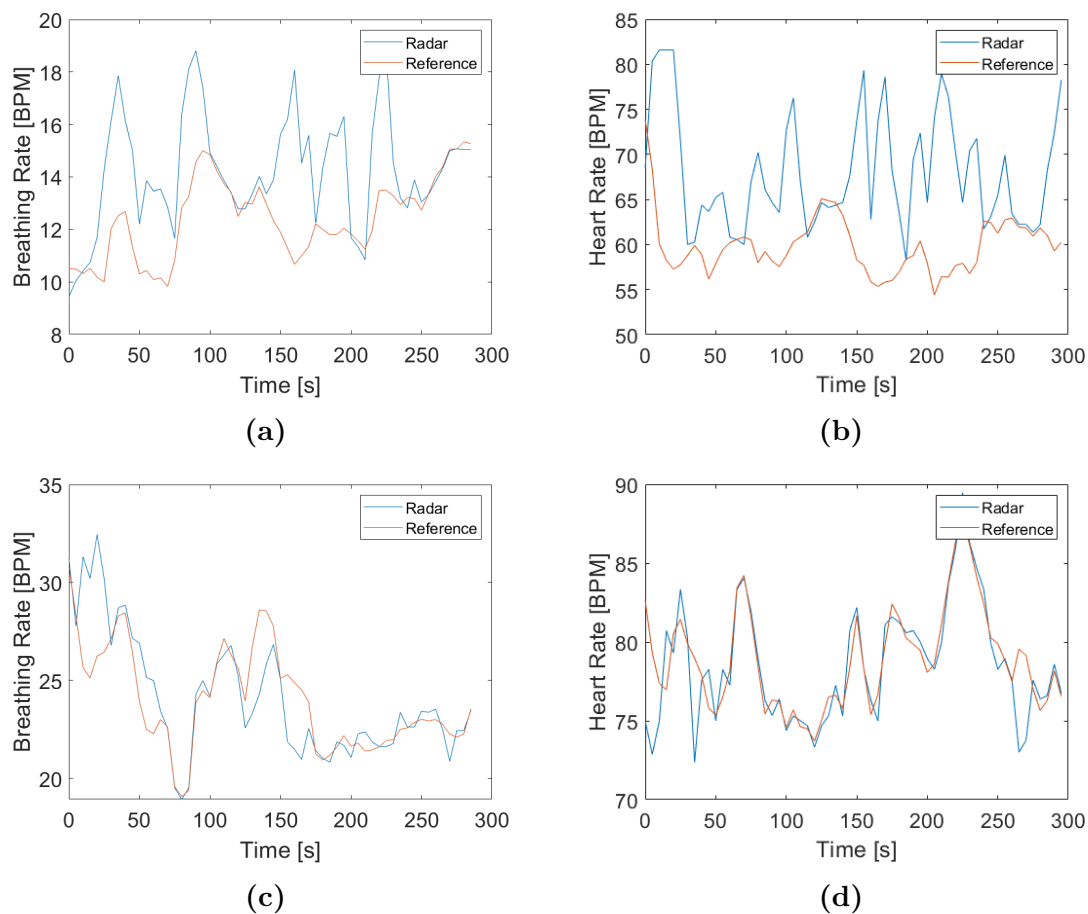


Figure 4.11: Average BR ((a) and (c)) and HR ((b) and (d)) for two test cases where the test subjects are sitting still. (a) and (b) are from the same test case, and the same applies for (c) and (d). Here, the wavelet method is used for signal processing.

Table 4.7: Summary of accuracy of signals shown in Figure 4.11, where the wavelet approach is used for signal processing.

Figure	BR Accuracy (%)		HR Accuracy (%)	
	mean	median	mean	median
(a) & (b)	83.2	90.2	85.4	88.5
(c) & (d)	95.2	98.1	98.4	99.3

When the wavelet approach is combined with the moving average filter, we instead get the results presented in Figure 4.12 and Table 4.8 for the same cases as described above. Note that, when comparing the two test cases in Figure 4.12 to each other ((a) & (b) compared to (c) & (d)), they both follow the reference quite well for both HR and BR. Further, also the accuracies are similar between the two cases.

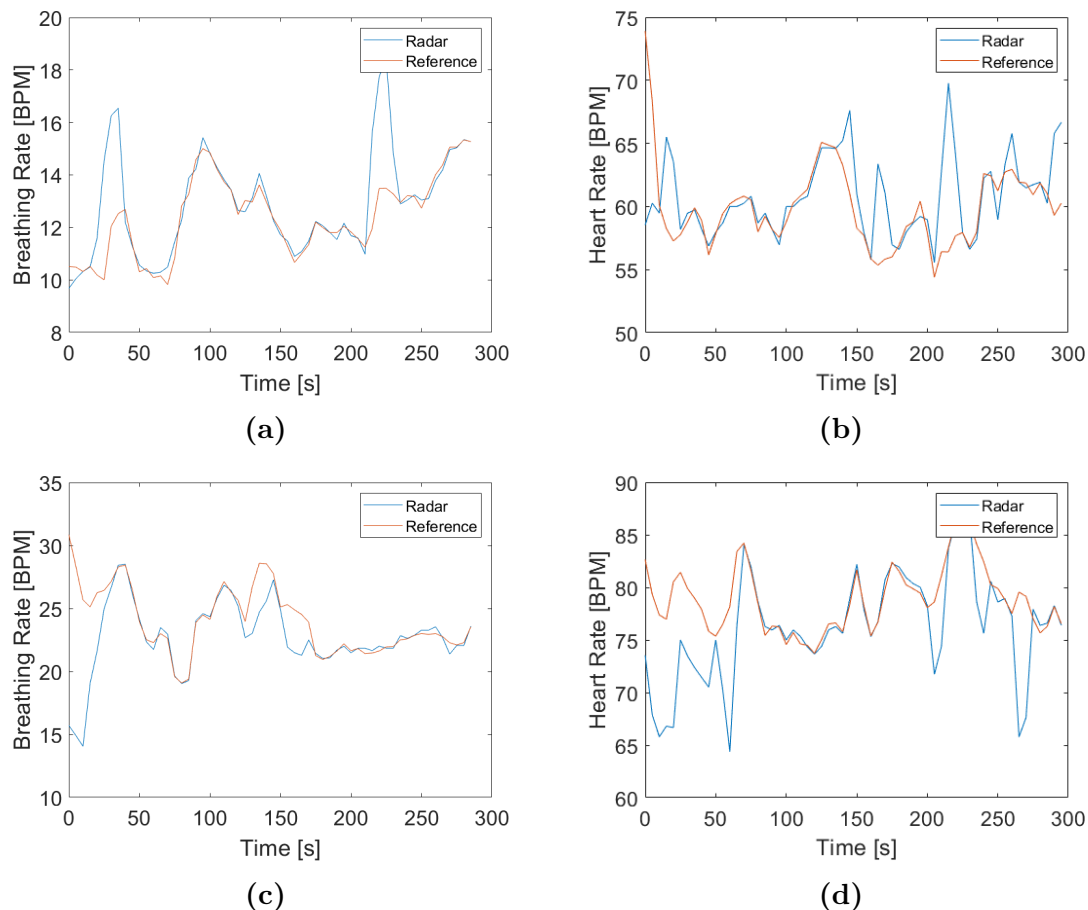


Figure 4.12: Average BR ((a) and (c)) and HR ((b) and (d)) for two test cases where the test subjects are sitting still. (a) and (b) are from the same test case, and the same applies for (c) and (d). Here, the signal processing is a combination of the wavelet approach and the moving average filter.

Table 4.8: Summary of accuracy of signals shown in Figure 4.12, where a combination of wavelets and moving average filters is used for signal processing.

Figure	BR Accuracy (%)		HR Accuracy (%)	
	mean	median	mean	median
(a) & (b)	94.4	98.5	96.5	99.0
(c) & (d)	94.5	99.0	96.2	99.3

These methods should be compared to the standard method used, which is the moving average approach used alone. The estimated HR and BR are presented in Figure 4.1, and corresponding accuracies in Table 4.9. When comparing these results to the results in Figure 4.12, where the combination of wavelets and the moving average filter was used, we see that they are similar. In the same way the accuracies for when using only the moving mean filter is similar to the accuracies in Table 4.8, where the combination of methods was used.

Table 4.9: Summary of accuracy on signals shown in Figure 4.1, where the moving average filter is used alone for the signal processing.

Figure	BR Accuracy (%)		HR Accuracy (%)	
	mean	median	mean	median
(a) & (b)	96.3	98.5	96.2	99.1
(c) & (d)	96.8	98.9	96.8	99.4

4.2.2 Cut-off Frequency of Band Pass Filter

The filtering to extract heartbeats from the radar signal includes a band pass filter, mainly used for baseline drift removal but also to suppress higher frequencies. However, the lower cut-off frequency of this filter also has an impact on the peak detection. Figure 4.13a shows the average HR for a case where the accuracy can be improved by changing the cut-off frequency to 0.8 Hz, instead of 0.6 Hz which is the standard value used. Here, the mean and median accuracies are 99.2% and 99.7%, respectively. This should be compared with Figure 4.1d showing the same case, but with the lower cut-off frequency. In that case the accuracies are 95.8% and 98.2% for mean and median, respectively. However, increasing the lower cut-off frequency is not always improving the results. In Figure 4.13b we see an example where the accuracy decreases when using the increased cut-off frequency. Here, the mean and median accuracies are 92.1% and 98.1%, which are to be compared with 98.7% and 99.5%, for the same case shown in Figure 4.1b. The only controlled difference between these cases is that there are two different subjects. Also, note that in Figure 4.13a the HR is significantly higher compared to Figure 4.13b.

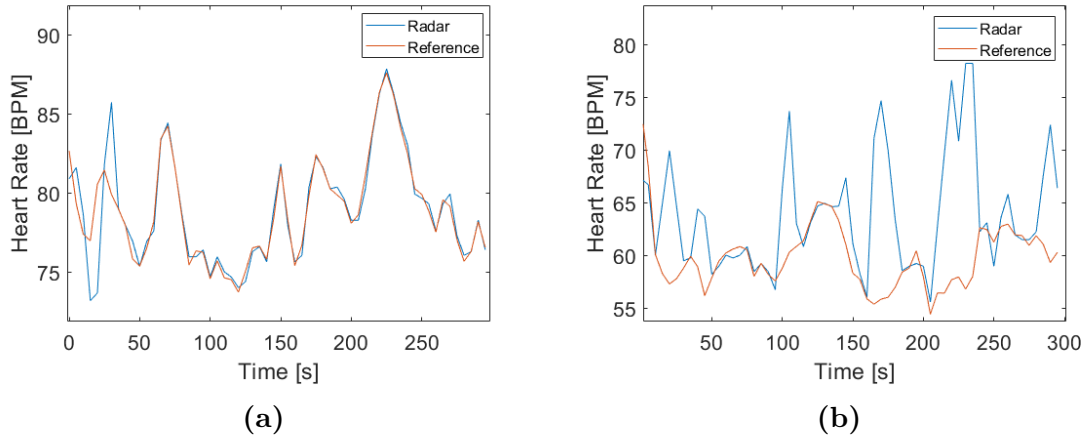


Figure 4.13: Average HR for two tests with different subjects, when the lower cut-off frequency in the band pass filter used for baseline drift removal, is set to 0.8 Hz. The subjects are sitting still, and there are no vibrations applied. The test cases are the same as in (a) Figure 4.1d, and (b) Figure 4.1b.

4.2.3 Performance of Linear Demodulation

As described in section 2.3.1 there are different methods to demodulate the I/Q data from the radar. In this project mainly the classic demodulation is used, but also the linear demodulation described in [12] was investigated. Figure 4.14 shows an example of a case where linear demodulation can be an advantage. A comparison between Figure 4.14a and Figure 4.2a, illustrates the difference between the two different demodulation methods. Both figures show the demodulated data from the same test case, where the test subject is sitting still and there are no vibrations applied. As seen in Figure 4.2a, using the classic demodulation results in a lot of jumps in the demodulated signal. Note that these jumps do not appear when the linear demodulation is used in Figure 4.14a. Also, as seen in Figure 4.15a, when linear demodulation is used, the estimated BR follows the reference much better compared to the results when classic demodulation is used, shown in Figure 4.15b. The mean accuracy is 95.7% when linear demodulation is used, whereas for the classic demodulation it is 90.0%. Moreover, in Figure 4.14b, the I and Q component of the linearly demodulated signal are shown. Note that both components have a similar variance.

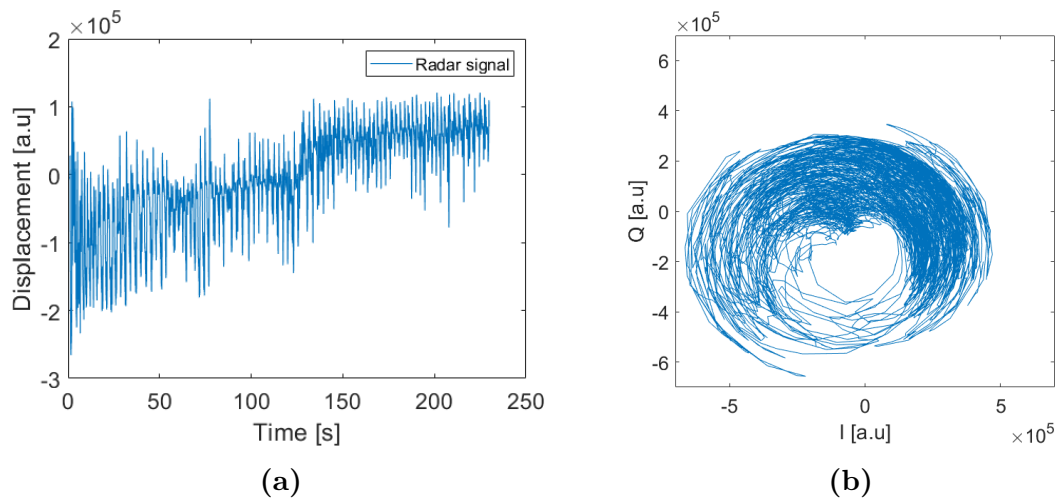


Figure 4.14: (a) Radar signal demodulated using linear demodulation, same data as in Figure 4.2a. (b) Corresponding linearly demodulated I/Q data.

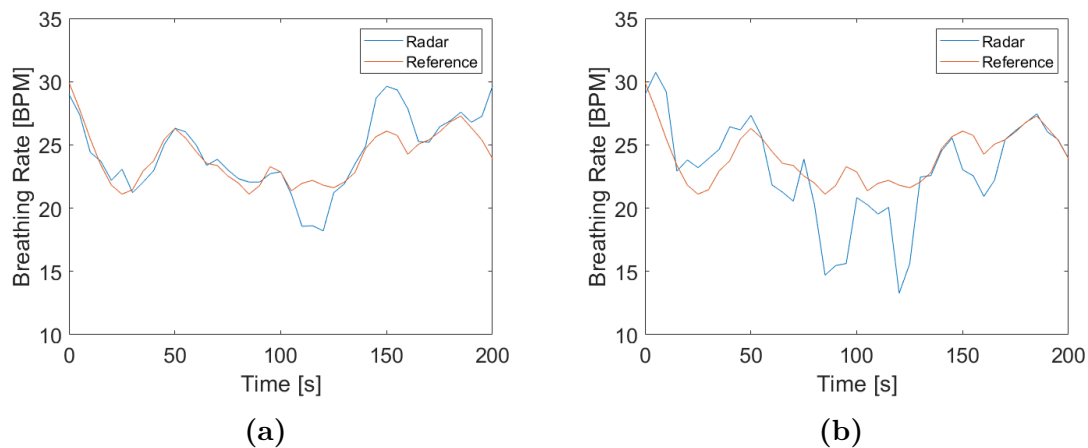


Figure 4.15: Estimated BR for the same test as shown in Figure 4.14 when using (a) linear demodulation, and (b) classic demodulation.

4.3 Additional Results

In this section a few less extensive, nevertheless important, results are presented. Beginning with presentation of initial results regarding heart sound detection, followed by a brief look at the data from the steering wheel.

4.3.1 Detection of Heart Sounds

The project included some initial evaluation of the possibility of detecting heart sounds using the same measuring setup as for the other measurements. Here, a higher sampling frequency was used, and the measured radar signal was band pass filtered around relevant heart sound frequencies. A part of a filtered heart sound

4. Results

signal is shown in Figure 4.16. This is for one of the cases with best signal quality. Note that the heart sounds are clearly visible in the filtered signal and that they match the reference.

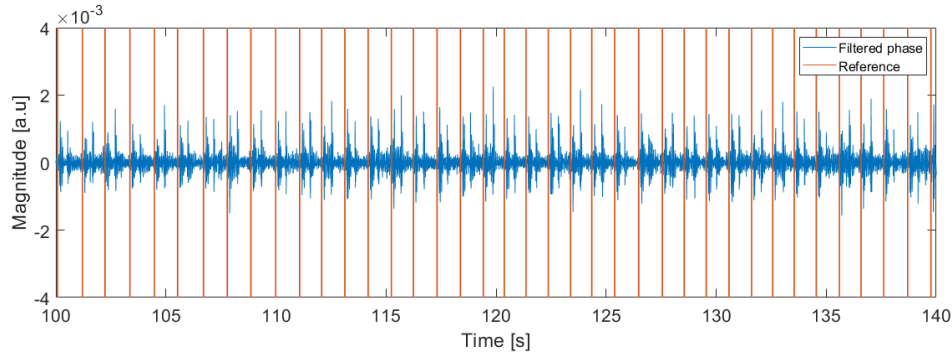


Figure 4.16: Heart sounds shown as a blue line. The red vertical lines are the reference ECG signal.

The first heart sound in each cardiac cycle was manually annotated and the IBI was calculated. Figure 4.17 shows the IBI of the heart sounds compared to the IBI of the reference ECG, for the signal shown in Figure 4.16. For this case the mean and median accuracies of the IBI are both 99.3 %.

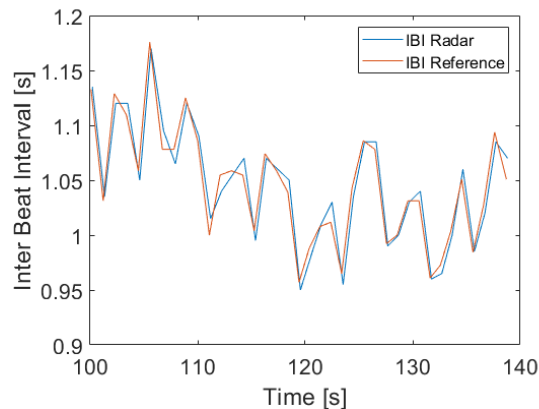


Figure 4.17: The IBI of the heart sounds and the reference ECG, for the measurement shown in Figure 4.16.

4.3.2 Steering Wheel Measurements

In the first data collection set half of the measurements were conducted from the steering wheel. However, as mentioned, due to time limitations it was decided to focus on the seat belt measurements. Therefore, the measurements from the steering wheel has just been briefly analysed. Figure 4.18 shows one of the measurements with highest accuracy values. For the BR the accuracies are 95.5 % in mean and 97.2 % in median, and the HR mean and median accuracies are 98.6 % and 99.3 %,

respectively. This is from a case where the subject sits still and there are no vibrations applied.

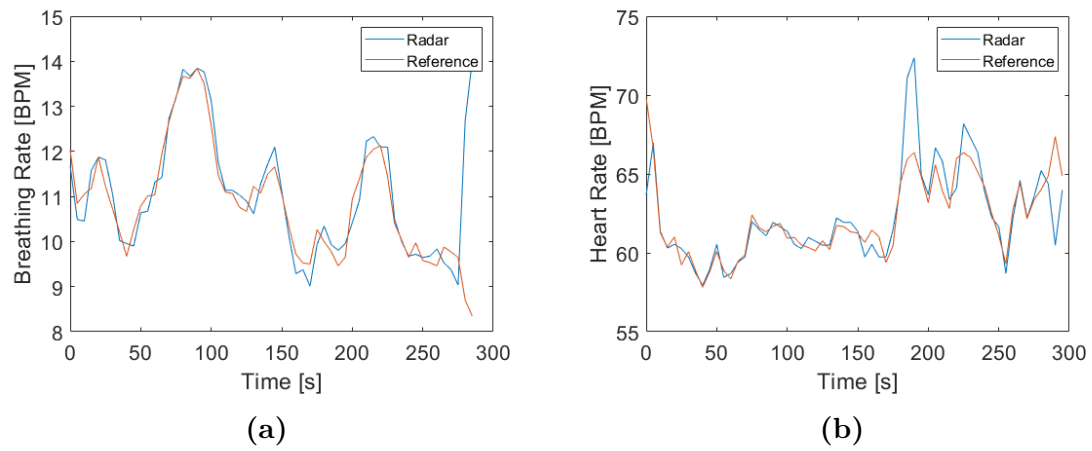


Figure 4.18: (a) Average BR and (b) HR from a measurement conducted from the steering wheel.

5

Discussion

In this chapter the results and the methodology of the project are discussed. First, an evaluation of the different test conditions and varied parameters are presented. This is followed by an analysis of the test setup and radar configuration, together with a discussion of possible areas of improvement. Further, we elaborate on the performance of the signal processing and a few potential signal processing approaches for the future. Lastly, we discuss relevant ethical considerations.

5.1 Evaluation of Different Test Conditions

The results presented in section 4.1 show that both the average BR and average HR can be detected accurately when the test subject sits still and there are no vibrations. The average of the mean accuracy for BR, presented in Table 4.2, is 92.9 %, which correspond to an absolute error of about 0.7-2.1 BPM, assuming a BR between 10-30 BPM. Note also that for many of the measurements the accuracy is even higher than the average, as best 96.8 %. Instead focusing on the HR, the average of the mean accuracy is 91.2 %, corresponding to an absolute error of 5.4-7.7 BPM, assuming a HR between 60-85 BPM. However, we can see in Table 4.2 that for the majority of the measurements, the mean HR accuracy is above 95 %. An accuracy of 95 % would instead correspond to an absolute error of 3-4.3 BPM. A possible explanation for the lower accuracy results could be a lower quality of the measured signal. As described in Figure 4.2, the quality of the measured signal varies. On the other hand, for the same test cases we manage to detect the BR quite accurately, which might suggest that the signal quality may not be the issue here, and that the lower accuracy is instead a result of the signal processing applied. However, more probably, the signal is good enough to resolve breathing, but not heartbeat. The breathing pattern is usually larger, and therefore it is easier to measure.

The results related to movements of the driver, presented in section 4.1.2, show that movements of the driver impose a great challenge. A comparison of BR accuracies for test with movements, in Table 4.3, with the ones without movements, presented in Table 4.2, show that movements result in a substantial decrease in accuracy. However, for the HR accuracy the results are not as clear. The average HR accuracies with movements are similar to the ones without movements. Note that the HR

accuracy do not change much between measurements in Table 4.3, resulting in a representative average. As discussed above, in Table 4.2 the average might not be representative for all of the measurements. An accuracy of 95 % might be a better value used for comparison. In that case, the decrease in accuracy due to movements is clear also for the HR. However, it is reasonable to think that movements will have a greater impact on the breathing measurements since the movements are relatively slow and low frequent. This would interfere more with the breathing, which consist of lower frequencies.

Another parameter that has been studied is the impact of vibrations. In section 4.1.3 we can see that, similar to body movements, adding vibrations generally result in lower accuracies. This is somewhat expected since vibrations lead to body movements and that affects the performance. The characteristics of the movements are somewhat different though. Vibrations are more likely to cause small movements with higher frequencies while steering movements are slower and larger movements. Evaluating the accuracies with vibrations, displayed in Table 4.4, we can see that they span a wide range, especially for the BR. However, the measurements resulting in the highest accuracies are in line with the ones without vibrations, showing great performance of our signal processing. This high performance is not seen for the steering movements, suggesting that vibrations might be less of a problem, or that our signal processing can handle vibrations in a better way. Anyhow, the consistency of the accuracies is still not very high. This is likely because of variations in the signal quality and hence, issues derived to the test setup. More about this is section 5.2.

The effects of talking are presented in section 4.1.4. When we talk, the breathing is different, which is clearly illustrated in Figure 4.8. During a conversation you normally talk for a short time and then listen to the answer. This cause rapid changes in the BR, as seen in Figure 4.9. Extracting an accurate BR during talking put higher demands on the signal processing, adapting to the rapid changes. Measuring the average BR when there are rapid changes might not be the best measure of the BR. We see in Table 4.5, showing the accuracies when talking, that our signal processing method has trouble to accurately detect the BR. The reason for this is not known but might be related to the signal processing we apply. It could also be that having a conversation cause other distortions to the signal. Every little motion such as a little sigh or laugh affect the signal, and this type of event might be more common during a conversation.

Further, it is also important to discuss if it is meaningful to measure the BR when the subject is talking. Maybe, it would be of more interest to identify when the subject is talking and not try to measure the BR. For the purpose of sleepiness detection, the information that the subject is talking may be more relevant than the exact BR.

In addition, looking at the HR accuracy we see that talking have a high impact on the performance here as well. In average, the mean accuracy is 90.8 %, corresponding

to an error of about 5.5-7.8 BPM for a HR between 60-85 BPM. This is similar to corresponding results with vibrations or steering movements. Another aspect of talking is that vibrations from the vocal cords might propagate through the body and cause distortion on the chest wall. This effect has not been studied further but could potentially affect the measured vibration of the chest wall and hence the result.

As described earlier, the measurements where the test subject wears a jacket are combined with vibrations and movements according to a predefined sequence. For shorter parts of these measurements, the subject is sitting still, allowing for an analysis of the effect of the jacket. By comparing the accuracies when wearing a jacket, in Table 4.6, and the ones with vibrations, in Table 4.4, we can see that the effect of the jacket is small. The accuracies for both BR and HR are similar to those with vibrations and thinner clothing. Note also that the highest accuracies with a jacket are in line with those without. Further, it should be noted that the amount of data for the case with a jacket are less than for other cases discussed above. A more extensive analysis of the effect of thicker clothing would need more data. However, the results presented here align well with theory outlined in section 2.2.1, which suggest that a thicker jacket does not pose a problem.

Another observation from the results is that in general the median accuracy is higher than the mean accuracy, both for BR and HR. The median as a metric is more robust against outliers than the mean. In our case, if the peak detection finds false peaks, or miss true peaks, then this will not have a great impact on the median, whereas the mean will immediately be reduced. If the median accuracy is high, then the performance of our signal processing is good for the majority of the time.

As a summary, we see that the applied signal processing allows accurate detection of average HR and BR when distortions are limited. A general observation, applying for all test cases, is that the robustness can be improved. The variation between different measurements is relatively high throughout all cases, which makes it complicated to draw general conclusions.

5.2 Analysis of Test Setup

Naturally, the test setup has a large impact of the measured signal, and in turn the possibility of achieving good results. Therefore, this section discusses some characteristics and suggestions of improvement of the test setup.

As pointed out in section 4.1.1, different measurements for the same test case can look quite different. For instance, Figure 4.2 shows four measurements for a case with the same stationary subject, with no movements and no vibrations applied. We can see that in Figure 4.2a there are a lot of jumps, which are not present to the same extent in the other measurements. These jumps can possibly be a result of small, but fast, movements of the subject. In the phase extraction such movements will be unwrapped, as described in 2.3.1.1. A phase shift of more than π rad between

two neighbouring samples will be unwrapped, since the algorithm assumes that the signal has been wrapped. However, notice that this assumption sometimes can be wrong, if the subject moves fast, but short. Here, this means a movement of 1 mm in 40 ms, which is the time between the chirps. This corresponds to a velocity of 0.03 m/s. Movements faster than this will cause a phase shift above π rad and result in unwrapping even though it should not. Looking at the signal, these movements appear as false jumps.

The small, fast movements can have some different explanations. For example, it can be the subject moving, but it can also be a result of the measurement setup. The current setup, which is described in section 3.2.1, uses a relatively large and heavy radar system mounted in a plastic box, which in turn is mounted on the seat belt. This setup makes it hard to ensure that the position of the radar is always the same, and also to make sure that the radar does not move during the measurements. As mentioned in section 3.2.1 the seat belt length was fixed, which made the setup more stable since it prevented the seat belt from hanging, but still the radar could move slightly. Especially when there are steering movements, it is challenging to keep the radar position stable. Worth considering, is that even in a real car setting, with the radar integrated in the seat belt, the driver and the seat belt could move a little relative to each other.

A way of handling the jumps in the signal could be by developing a suitable signal processing method that in a way can handle or avoid them. An example is the linear demodulation approach, described in [12], which was also explored in this project. Figure 4.14a shows the results for when the same measurement as in Figure 4.1a, with all the jumps, was instead linearly demodulated. We see clearly that now the jumps are not present in the signal. We also see that the BR mean accuracy increases and that the estimated average BR in Figure 4.15a follows the reference quite well. Note that this method does not use the unwrapping, which is the explanation to why the jumps disappear. However, it is also important to notice that this method does not use all the data and therefore there will be some loss of information in the demodulated data. Looking at Figure 4.14b we see that there is quite much information in both I and Q direction. Hence, since the linear demodulation uses only information in either I or Q direction, rather much information will be lost. In the particular case shown in this example, the linear demodulation is an advantage despite the loss of information, since the classic demodulation did not work well here. Nevertheless, for other cases, where the classic demodulation works well, the loss of information may be a larger problem.

One way of finding a more stable position of the radar may be to place it in the steering wheel instead. In section 4.3.2 we present some measurements from this setup. The results are quite promising, at least for the stationary case, without body movements and vibrations. With this setup the weight of the radar is not a problem in the same way, but we instead introduce some other potential problems. For example, objects in the surroundings, and the steering movements of the arms, can distort the measured signal. In addition, the steering wheel will be turning in a

real car setting, which will complicate the signal processing and also the technical design further.

Another possible position of the radar is in the backrest of the seat, measuring the movements of the back due to heartbeats and breathing, as described in [8]. A benefit from this position is that the back is usually resting against the seat, which could result in less movements that corrupts the signal. On the other hand, the signal strength from this position might be reduced, since the breathing and heartbeat movements of the back are smaller, compared to the chest. However, this position was not tried out in this project since the focus was to investigate positions of interest for Autoliv products.

In addition, the use of a vibration rig and the reliability of the vibrations should be discussed. After all, the vibration rig is a model of the reality and it is of interest to verify that it is a realistic model. This is important in order to know if the results presented in this thesis is transferable to a real driving scenario. One part of this would be to analyse the vibrations. As mentioned earlier, the vibration data are heavily down sampled and the effect of this should be further investigated.

Finally, also the effects of the plastic shielding in front of the radar should be considered. Some simpler tests were done to ensure that measurements could be performed using the cover. Even with the cover on, the displacements of the chest wall were visible in the signal. However, it could potentially affect the behaviour of the measured signal, for instance by causing reflections of the signal within the cover. Moreover, as mentioned in section 3.2.1, the plastic cover creates an air gap between the radar sensor and the body. This air gap is essential to be able to measure the chest wall displacements, but it probably does not need to be as large as the gap caused by the cover. Some simpler test where the radar was held closer to the chest, without the cover, were done with good results. This is promising for a future integration in the seat belt, but this topic could benefit from more research.

5.3 Hardware and Radar Configuration

In this project, the configuration of the radar, such as the sampling frequency and the bandwidth of the chirps, described in section 2.1, were set based on some initial testing to get a high quality signal. In this section we discuss some of the parameters and the hardware designs that could benefit from further research.

First, the bandwidth of the chirp is important for the signal behaviour and is also directly connected to the range resolution of the measured signal. A shorter bandwidth results in a lower range resolution, and hence larger range bins. Based on some initial testing, the bandwidth in this project is set to 3.4 GHz, to get a high quality signal. This corresponds to range bins of about 4 cm, which should be considered as quite short. An advantage of this is that the signal from each bin only has contribution of reflections from a small range, and therefore also the contribution of noise is reduced. However, the small range bins can also be somewhat troublesome

when selecting the range bin to analyse. Since the radar transmits its signal in a lobe, the signal will be reflected on different parts of the chest wall, and the reflected signal will be present in many range bins. This could motivate to use larger range bins, as in [8], [12]. On the other hand, if the range bin is selected correctly, the signal quality might be higher when using smaller range bins.

Further, the sampling frequency of the phase signal was set to 25 Hz (each chirp was sent out every 40 ms) for all measurements except for the heart sounds. Hence, frequencies up to 12.5 Hz can be measured, according to the Nyquist theorem. This should be enough to measure HR and BR, based on the normal frequency ranges [14]. However, a higher sampling frequency could possibly reduce some of the problems with body movements. As described in section 5.2, fast movements can cause false jumps in the signal. This is related to the sampling frequency, since the movements causing the jumps are movements larger than 1 mm between two samples. With a higher sampling frequency, the movements then has to be faster to cause the jumps.

Another configuration option that could be of interest for further research is the number of antennas used. Using more antennas enables to direct the lobe of the radar more, and in that way have more control of the measurement. Maybe this could also be used to facilitate the selection of range bins, while still using small range bins to avoid unnecessary noise.

Finally, for a real application, and maybe also for further investigation, the radar system design has to be considered. It would be an advantage for the test setup if the radar system was lighter and smaller, so that it can be mounted more stable. It is also important to consider the radiated power from the radar, so that requirements of regulations are fulfilled. This is further discussed in section 5.7.

5.4 Individual Differences Between Subjects

When measuring physiological signals, it is reasonable to discuss some individual differences. We all have different breathing and heartbeat patterns, which puts high demands on the signal processing since it must adopt to the test subject. This has been a challenge throughout this project and handling individual differences during signal processing is further elaborated in section 5.6.

The signal that we measure has its origin in vibrations of the chest wall and it is reasonable to think that there is an individual aspect to these vibrations as well. Aspects such as body shape and fitness level, as well as anatomical differences could potentially affect the signal quality. Further, anatomical differences are to some extent governed by the gender, which may have an impact when measuring at the chest position. However, in this project, the results have been similar for both test subjects, which are of different gender.

Another relevant aspect is how we breathe, which may differ from person to person, but also from time to time. Breathing can be shallow and with short breaths, but

also longer, deeper breaths can occur. This will of course affect the measured signal and the quality of it. It could be of interest to investigate the signal quality from different locations further, and also to see if BR and HR should be measured from the same location. It is not self-evident that they must be measured at the same location, even if it is convenient and cost-effective to use the same device.

5.5 Feasibility of Measuring Heart Sounds

The results presented in section 4.3.1 show great potential in detecting heart sounds. One of the good signal segments have been selected, clearly illustrating the feasibility of detecting heart sounds. In Figure 4.17 the IBI for the reference and radar signal is very similar, which is also reflected in the accuracy of 99.3%. This suggest that heart sound present an opportunity to not only detect the HR but also HRV. However, a more extensive analysis of the robustness to distortions is needed, as well as further development of the signal processing. As mentioned before, the heart sounds are manually annotated in this project and further research should focus on doing this automatically.

5.6 Discussion of Signal Processing

Over the course of this project a few different signal processing approaches has been tested. In section 4.2.1 a comparison of the use of wavelets and moving average filtering is shown. In general, it has been troublesome to choose one generic signal processing technique that consistently produce good results. The idea to use wavelets was inspired by previous research, showing promising results [8], [12]. But as described in section 4.2.1, the results were improved when adding a moving average filter. However, excluding the wavelet method and only use the moving average filter turned out to yield similar results. Suggesting that using the wavelet method is redundant.

Nonetheless, we still think that using wavelets could be a possible solution to extract BR and HR, and suppress noise, but a deeper knowledge and understanding of the method is needed. In order to further develop the method, a more extensive analysis of the noise should be done. With more knowledge of what information can be discarded, the choice of wavelet, levels and associated threshold could be designed accordingly.

Another challenge with regards to signal processing is how to handle individual differences. In section 4.2.2 the issue of designing a band pass filter to fit different test subjects is described. The lower cut-off frequency of the band pass filter used to extract the heartbeat signal has a great impact on the result. This is due to the fact that one of the test subjects has a lower resting HR than the other. We can see in Figure 4.13b that the HR fluctuates around 60 BPM, equivalent to 1 Hz. A cut-off frequency of 0.8 Hz in that case cause a loss of information that strongly affect the result. However, in Figure 4.13a, the HR are higher, around 80 BPM, and there the

cut-off frequency at 0.8 Hz result in better accuracy, since more of the irrelevant parts are attenuated.

These results highlight the challenge of individual differences and that the results can be improved by adjusting the signal processing from case to case. With this in mind, we think that there is a need for an adaptive signal processing. For this, a band pass filter might not be optimal. In the following section, a few signal processing ideas are presented.

5.6.1 Future Signal Processing

There are several signal processing techniques that have been discussed during the project, but not implemented. One of these is the use of neural networks to find and classify peaks. The concept is to use the reference signal to find the true peaks. These can then be used to train the neural network to detect the correct peaks in the radar signal. In order for this to work, the reference and radar signal would need a more exact synchronisation than in this project and more data from different test subjects. This has not been tested during this project due to time limitations.

Another technique that could be utilised is differentiation. By differentiating the measured signal, peaks can be enhanced, and the idea is to enable a more accurate peak detection. Related to this, instead of detecting peaks, a template based peak detection, described in [30] could be of interest. The idea is to find a set of templates, representing different shapes of the heartbeat signal during a training stage. These templates can then be used to find the location of heartbeats.

Moreover, in this project, the BR and HR were calculated for all measured data, independently of the signal quality. Therefore, the calculated BR and HR sometimes is very different from the reference data. This might be a problem in a real application, where the calculated data should be used for estimating the sleepiness. An idea to avoid this, would be to have a measure of the quality of the signal or the calculated results. This could then be used to determine which parts of the data that should be used for estimating the sleepiness.

5.7 Ethical Considerations

Millimeter wave (mmWave) radiation is non-ionizing electromagnetic radiation with high frequency [31], [32]. The main safety concern is heating of the skin and eyes due to absorption of the mmWaves in the human body, and very high power of mmWave radiation can cause burns [32]. To avoid harmful effects there is an European exposure limit for the power density that is 10 W/m^2 [33]. The radar sensor used in this project has, according to the manufacturer, equivalent isotropic radiated power (EIRP) of at maximum 400 mW, and the European exposure limit is fulfilled if the distance between the sensor and the subject is at least 5 cm [34]. In order to measure from a seat belt position the radar must be placed closer than 5 cm to the subject. Considering reflections from clothing it is unlikely that the

power reaching the subject will be harmful. This assumption is based on the fact that the radiated power from a mobile phone, a device that is used daily, is 1-2 W [35]. Further, the subjects in this project will only be exposed during a short period of time. In future implementations and possibly commercial applications, this issue must be investigated further.

Further, since the radar equipment was placed between the seat belt and the chest wall of the driver, it was considered as a safety risk in case of an emergency. Therefore, the data collection was performed using a vibration rig, and the data collection is then not considered as a large risk for the subject.

Data concerning a person's health condition is considered as sensitive personal data and is therefore covered by the General Data Protection Regulation (GDPR) [36]. Thus, data collection of vital signs requires the person's explicit consent. This did not cause any problems in this particular project, since the data was only be collected from ourselves, and we had given our consent.

6

Conclusion

The results of this project show promising results for driver monitoring using radar technology. With an FMCW radar sensor attached to the seat belt, accurate detection of BR and HR were achieved under stationary condition. Although vibrations from the car affect the performance, successful detection can still be obtained for some measurements. Body movement and talking turn to be the major problem, and have big impact on the detection accuracy.

We conclude that further efforts are needed to ensure a high quality signal measurement. In this project, the varying signal quality is mainly attributed to the unstable test setup. Further investigation of the applicability of the vibration rig and testing in a real car is needed in order to strengthen our results. Also, we suggest that resources are dedicated to developing a radar device tailored to this application, enabling a more stable mounting.

For the breathing signal, we conclude that removing the baseline drift and applying a moving average filter enables accurate detection of the average BR. Similarly, for the heartbeat signal, a windowed band pass filter accompanied with a moving average filter results in decent accuracy for the average HR. The wavelet method tested to extract breathing and heartbeats do not increase the overall performance. However, we do think that the use of wavelets has potential if the method is refined. One issue with the signal processing used is the adaptivity to individual subjects. Therefore, future development is suggested to focus on a more adaptive signal processing.

References

- [1] World Health Organisation, *Global status report on road safety 2018*. [Online]. Available: <https://www.who.int/publications-detail-redirect/9789241565684> (visited on 01/29/2021).
- [2] Statens väg- och transportforskningsinstitut, *Trötthet hos förare*. [Online]. Available: <https://www.vti.se/forskning/trafiksakerhet/trotthet-hos-forare> (visited on 01/29/2021).
- [3] National Highway Traffic Safety Administration, *Drowsy Driving*. [Online]. Available: <https://www.nhtsa.gov/risky-driving/drowsy-driving> (visited on 01/29/2021).
- [4] European Commission. (Jul. 5, 2016). “Safety in the automotive sector,” Internal Market, Industry, Entrepreneurship and SMEs - European Commission, [Online]. Available: https://ec.europa.eu/growth/sectors/automotive/safety_en (visited on 05/20/2021).
- [5] A. Čolić, O. Marques, and B. Furht, *Driver Drowsiness Detection: Systems and Solutions*, ser. SpringerBriefs in Computer Science. Springer International Publishing, 2014, ISBN: 978-3-319-11535-1. DOI: 10.1007/978-3-319-11535-1_1.
- [6] F. Guede-Fernandez *et al.*, “Driver Drowsiness Detection Based on Respiratory Signal Analysis,” *IEEE Access*, vol. PP, Jun. 2019. DOI: 10.1109/ACCESS.2019.2924481.
- [7] M. Kebe *et al.*, “Human Vital Signs Detection Methods and Potential Using Radars: A Review,” *Sensors (Basel, Switzerland)*, vol. 20, no. 5, Mar. 2020, ISSN: 1424-8220. DOI: 10.3390/s20051454.
- [8] I. D. Castro *et al.*, “Physiological Driver Monitoring Using Capacitively Coupled and Radar Sensors,” *Applied Sciences*, vol. 9, no. 19, Jan. 2019. DOI: 10.3390/app9193994.
- [9] C. Will *et al.*, “Radar-Based Heart Sound Detection,” *Scientific Reports*, vol. 8, no. 1, Jul. 2018, ISSN: 2045-2322. DOI: 10.1038/s41598-018-29984-5.
- [10] Chalmers University of Technology, *Tekniken som märker om du dåsar till bakom ratten*. [Online]. Available: <https://www.chalmers.se/sv/institutioner/e2/nyheter/Sidor/Tekniken-som-marker-om-du-dasar-till-bakom-ratten.aspx> (visited on 04/08/2021).
- [11] S. Rao, “Introduction to mmwave Sensing: FMCW Radars,” p. 70, [Online]. Available: https://training.ti.com/sites/default/files/docs/mmwaveSensing-FMCW-offlineviewing_2.pdf (visited on 02/01/2021).

- [12] M. Mercuri *et al.*, “Vital-sign monitoring and spatial tracking of multiple people using a contactless radar-based sensor,” *Nature Electronics*, vol. 2, no. 6, pp. 252–262, Jun. 2019, ISSN: 2520-1131. DOI: 10.1038/s41928-019-0258-6. [Online]. Available: <http://www.nature.com/articles/s41928-019-0258-6> (visited on 02/16/2021).
- [13] A. D. Droitcour, “Non-contact measurement of heart and respiration rates with a single-chip microwave doppler radar,” PhD. Thesis, Department of Electrical Engineering, Stanford University, Stanford, USA, 2006. [Online]. Available: <http://citeseerx.ist.psu.edu/viewdoc/download?doi=10.1.1.84.7516&rep=rep1&type=pdf> (visited on 02/20/2019).
- [14] I.-Q. Chung, J.-T. Yu, and W.-C. Hu, “Estimating Heart Rate and Respiratory Rate from a Single Lead Electrocardiogram Using Ensemble Empirical Mode Decomposition and Spectral Data Fusion,” en, *Sensors*, vol. 21, no. 4, p. 1184, Jan. 2021. DOI: 10.3390/s21041184.
- [15] T. Noto *et al.*, “Automated analysis of breathing waveforms using BreathMetrics: A respiratory signal processing toolbox,” en, *Chemical Senses*, vol. 43, no. 8, Sep. 2018, ISSN: 0379-864X. DOI: 10.1093/chemse/bjy045.
- [16] H. Kaneko and J. Horie, “Breathing Movements of the Chest and Abdominal Wall in Healthy Subjects,” en, *Respiratory Care*, vol. 57, no. 9, Sep. 2012, ISSN: 0020-1324, 1943-3654. DOI: 10.4187/respcare.01655.
- [17] L. M. Biga *et al.*, “19.3 Cardiac Cycle,” en, in *Anatomy & Physiology*, OpenStax/Oregon State University, 2019. [Online]. Available: <https://open.oregonstate.edu/aandp/chapter/19-3-cardiac-cycle/> (visited on 03/12/2021).
- [18] Ø. Aardal *et al.*, “Chest movement estimation from radar modulation caused by heartbeats,” in *2011 IEEE Biomedical Circuits and Systems Conference (BioCAS)*, Nov. 2011, pp. 452–455. DOI: 10.1109/BioCAS.2011.6107825.
- [19] T. Wu, T. S. Rappaport, and C. M. Collins, “The human body and millimeter-wave wireless communication systems: Interactions and implications,” en, in *2015 IEEE International Conference on Communications (ICC)*, London: IEEE, Jun. 2015, pp. 2423–2429, ISBN: 978-1-4673-6432-4. DOI: 10.1109/ICC.2015.7248688.
- [20] S. Dhupkariya, V. K. Singh, and A. Shukla, “A Review of Textile Materials for Wearable Antenna,” en, p. 10, 2014.
- [21] J. Skaar, “Fresnel equations and the refractive index of active media,” *Physical Review E*, vol. 73, no. 2, p. 026605, Feb. 2006. DOI: 10.1103/PhysRevE.73.026605.
- [22] S. Yamada, “Quadrature Radar Demodulation Techniques For Accurate Displacement Detection,” p. 82, 2016. [Online]. Available: https://scholarspace.manoa.hawaii.edu/bitstream/10125/51625/2016-12-phd-yamada.pdf?fbclid=IwAR09b1jKae6CfhnLceAkQ6QkHCOxiP6Jyi3gE79hXgS_LDAfCRg9oAyDTQQ (visited on 05/10/2021).
- [23] M. Misiti *et al.*, *Wavelet Toolbox User’s Guide*, en, 2009.
- [24] A. B. Romeo, C. Horellou, and J. Bergh, “A wavelet add-on code for new-generation N-body simulations and data de-noising (JOFILUREN),” en, *Monthly Notices of the Royal Astronomical Society*, vol. 354, no. 4, pp. 1208–1222, Nov. 2004, ISSN: 0035-8711, 1365-2966. DOI: 10.1111/j.1365-2966.2004.08303.x.

-
- [25] Texas Instruments, *AWR1642BOOST Evaluation board* / *TI.com*. [Online]. Available: <https://www.ti.com/tool/AWR1642BOOST#overview> (visited on 01/28/2021).
- [26] —, *DCA1000EVM Evaluation board* / *TI.com*. [Online]. Available: <https://www.ti.com/tool/DCA1000EVM> (visited on 01/28/2021).
- [27] Mind Media B.V, *NeXus-10 MKII* / *Biofeedback and neurofeedback device - Mind Media*. [Online]. Available: <https://www.mindmedia.com/en/products/nexus-10-mkii/> (visited on 04/06/2021).
- [28] Mind Media B.V, The Netherlands, *NeXus-10 MKII*, www.mindmedia.com.
- [29] J.-Y. Kim *et al.*, “Peak Detection Algorithm for Vital Sign Detection Using Doppler Radar Sensors,” *Sensors*, vol. 19, no. 7, p. 1575, Apr. 1, 2019, ISSN: 1424-8220. DOI: 10.3390/s19071575. [Online]. Available: <https://www.mdpi.com/1424-8220/19/7/1575> (visited on 03/31/2021).
- [30] C. Will *et al.*, “Advanced template matching algorithm for instantaneous heartbeat detection using continuous wave radar systems,” in *2017 First IEEE MTT-S International Microwave Bio Conference (IMBIOC)*, IEEE, May 2017, pp. 1–4, ISBN: 978-1-5386-1713-7. DOI: 10.1109/IMBIOC.2017.7965797. [Online]. Available: <http://ieeexplore.ieee.org/document/7965797/> (visited on 04/06/2021).
- [31] T. Wu, T. S. Rappaport, and C. M. Collins, “The human body and millimeter-wave wireless communication systems: Interactions and implications,” in *2015 IEEE International Conference on Communications (ICC)*, Jun. 2015, pp. 2423–2429. DOI: 10.1109/ICC.2015.7248688.
- [32] T. Wu, T. S. Rappaport, and C. M. Collins, “Safe for Generations to Come,” *IEEE microwave magazine*, vol. 16, no. 2, pp. 65–84, Mar. 2015, ISSN: 1527-3342. DOI: 10.1109/MMM.2014.2377587.
- [33] C. Oladimeji, “TI mmWave Radar Device Regulatory Compliance Guide,” p. 6, 2019.
- [34] Texas Instruments, “AWR1642 Evaluation Module (AWR1642BOOST) Single-Chip mmWave Sensing Solution,” p. 19, 2017.
- [35] G. J. Hyland, “Physics and biology of mobile telephony,” *Lancet*, vol. 356, no. 9244, pp. 1833–1836, Nov. 2000, ISSN: 00995355. DOI: 10.1016/S0140-6736(00)03243-8.
- [36] *Art. 9 GDPR – Processing of special categories of personal data*. [Online]. Available: <https://gdpr-info.eu/art-9-gdpr/> (visited on 01/29/2021).

A

Summary of Data Collections

The test cases from the first and second data collection are presented in Table A.1 and A.3, respectively. For the first data collection a sequence with events was used. This is summarised in Table A.2.

Table A.1: Summary of test cases for the first data collection.

Test Number	Test Subject	Antenna Position	Vibration Data	Clothing	Schedule
1	X	Steering Wheel	Motorway	Normal	No
2	X	Steering Wheel	Motorway	Normal	Yes
3	X	Steering Wheel	Motorway	Jacket	Yes
4	X	Steering Wheel	City Traffic	Normal	Yes
5	X	Steering Wheel	None	Normal	Yes
6	Y	Steering Wheel	Motorway	Normal	No
7	Y	Steering Wheel	Motorway	Normal	Yes
8	Y	Steering Wheel	Motorway	Jacket	Yes
9	Y	Steering Wheel	City Traffic	Normal	Yes
10	Y	Steering Wheel	None	Normal	Yes
11	X	Seat Belt	Motorway	Normal	No
12	X	Seat Belt	Motorway	Normal	Yes
13	X	Seat Belt	Motorway	Jacket	Yes
14	X	Seat Belt	City Traffic	Normal	Yes
15	X	Seat Belt	None	Normal	Yes
16	Y	Seat Belt	Motorway	Normal	No
17	Y	Seat Belt	Motorway	Normal	Yes
18	Y	Seat Belt	Motorway	Jacket	Yes
19	Y	Seat Belt	City Traffic	Normal	Yes
20	Y	Seat Belt	None	Normal	Yes
21	X	Steering Wheel	None	Normal	No
22	Y	Steering Wheel	None	Normal	No
23	X	Seat Belt	None	Normal	No
24	Y	Seat Belt	None	Normal	No

Table A.2: Sequence with events, applied during first test collection.

Time (s)	Event
0-90	Sit still
90-150	Small steering movements
150-180	Sit still
180-210	Say the days of the week once, then sit still
210-240	Adjust the seating position, then sit still
240-300	Simulate a roundabout, then sit still
300	End of recording

Table A.3: Summary of test cases for the second data collection.

Test Number	Test Subject	Antenna Position	Vibration Data	Talking	Steering Movements
1	X	Seat Belt	No	No	No
2	X	Seat Belt	No	No	No
3	X	Seat Belt	No	No	No
4	X	Seat Belt	No	No	Yes
5	X	Seat Belt	No	No	Yes
6	X	Seat Belt	No	Yes	No
7	X	Seat Belt	No	Yes	No
8	X	Seat Belt	Motorway	No	No
9	X	Seat Belt	Motorway	No	No
10	X	Seat Belt	Motorway	No	No
11	X	Seat Belt	No	No	No
12	X	Seat Belt	No	No	No
13	Y	Seat Belt	No	No	No
14	Y	Seat Belt	No	No	No
15	Y	Seat Belt	No	No	No
16	Y	Seat Belt	No	No	Yes
17	Y	Seat Belt	No	No	Yes
18	Y	Seat Belt	No	Yes	No
19	Y	Seat Belt	No	Yes	No
20	Y	Seat Belt	Motorway	No	No
21	Y	Seat Belt	Motorway	No	No
22	Y	Seat Belt	Motorway	No	No
23	Y	Seat Belt	No	No	No
24	Y	Seat Belt	No	No	No
25	X	Seat Belt	No	No	No
26	X	Seat Belt	Motorway	No	No
27	Y	Seat Belt	No	No	No
28	Y	Seat Belt	No	No	No

DEPARTMENT OF ELECTRICAL ENGINEERING
CHALMERS UNIVERSITY OF TECHNOLOGY
Gothenburg, Sweden
www.chalmers.se



CHALMERS
UNIVERSITY OF TECHNOLOGY